DTIC FILE COPY

4

TECHNICAL REPORT BRL-TR-2980

BRL

STRESS WAVES THROUGH PROJECTILE JOINTS AND
INTERFACES

JAMES M. BENDER

DTIC
ELECTE
SEP 13 1989
S E D

JANUARY 1989

APPROVED FOR PUBLIC RELEASE; DISTRIBUTION UNLIMITED.

U.S. ARMY LABORATORY COMMAND

BALLISTIC RESEARCH LABORATORY

ABERDEEN PROVING GROUND, MARYLAND

89 9 12 059

REPORT DOCUMENTATION PAGE		Form Approved OMB No. 0704-0188

1a. REPORT SECURITY CLASSIFICATION UNCLASSIFIED	1b. RESTRICTIVE MARKINGS

2a. SECURITY CLASSIFICATION AUTHORITY	3. DISTRIBUTION/AVAILABILITY OF REPORT APPROVED FOR PUBLIC RELEASE; DISTRIBUTION UNLIMITED
2b. DECLASSIFICATION/DOWNGRADING SCHEDULE	

4. PERFORMING ORGANIZATION REPORT NUMBER(S) BRL-TR-2980	5. MONITORING ORGANIZATION REPORT NUMBER(S)

6a. NAME OF PERFORMING ORGANIZATION USA Ballistic Research Lab	6b. OFFICE SYMBOL (If applicable) SLCBR-IB-M	7a. NAME OF MONITORING ORGANIZATION

6c. ADDRESS (City, State, and ZIP Code) Aberdeen Proving Ground, MD 21005-5066	7b. ADDRESS (City, State, and ZIP Code)

8a. NAME OF FUNDING/SPONSORING ORGANIZATION	8b. OFFICE SYMBOL (If applicable)	9. PROCUREMENT INSTRUMENT IDENTIFICATION NUMBER

8c. ADDRESS (City, State, and ZIP Code)	10. SOURCE OF FUNDING NUMBERS			
	PROGRAM ELEMENT NO.	PROJECT NO.	TASK NO.	WORK UNIT ACCESSION NO.

11. TITLE (Include Security Classification)

Stress Waves Through Projectile Joints and Interfaces

12. PERSONAL AUTHOR(S)
Bender, James M.

13a. TYPE OF REPORT	13b. TIME COVERED FROM _____ TO _____	14. DATE OF REPORT (Year, Month, Day)	15. PAGE COUNT

16. SUPPLEMENTARY NOTATION

17. COSATI CODES			18. SUBJECT TERMS (Continue on reverse if necessary and identify by block number)
FIELD	GROUP	SUB-GROUP	

19. ABSTRACT (Continue on reverse if necessary and identify by block number)

This report contains the results of studies of the response of a hollow cylinder containing a threaded joint to stress waves using the finite element method of dynamic stress analysis. These types of joints are very common in many current cargo-carrying artillery projectiles. Sharp rise-time loads, which generate stress waves, can occur with electromagnetic launch and can ocassionally result from a poorly behaved chemical charge (solid and liquid propellant) which creates pressure waves.

The joint studied in this report has two types of discontinuities. The first is a change of medium: the interface between aluminum and steel; and the other is a non-closing gap, typically found at a cylindrical joint with two closing faces.

20. DISTRIBUTION/AVAILABILITY OF ABSTRACT ☐ UNCLASSIFIED/UNLIMITED ☒ SAME AS RPT. ☐ DTIC USERS	21. ABSTRACT SECURITY CLASSIFICATION
22a. NAME OF RESPONSIBLE INDIVIDUAL James M. Bender	22b. TELEPHONE (Include Area Code) (301) 278-6116	22c. OFFICE SYMBOL SLCBR-IB-M

DD Form 1473, JUN 86   *Previous editions are obsolete.*   SECURITY CLASSIFICATION OF THIS PAGE

19. Abstract - cont'd

First, an analysis of a bi-metallic rod is performed to verify certain aspects of the finite element code such as time step, element size and type, and analysis type. Also, the response of a rod to stress waves can be easily compared to well-known analytical predictions.

Next, a hollow homogeneous cylinder is analyzed for the purpose of evaluating radial motion induced by the forcing function. This oscillatory motion disturbs the uniformity of the stress patterns. Only the initial pass of the stress wave is clear, and is similar in appearance to that of the rod. Thereafter, stress gradients through the wall thickness are evident with the onset of vibration modes, excited by the short-duration forcing function, appear to be a function of the duration of the applied transient load. Longer duration applied loads excite lower frequency modes.

Next, a non-closing notch discontinuity is introduced at the mid-section of the hollow cylinder. The stress transmitted through this discontinuity is determined for various notch depths and locations.

Finally, three configurations of the bi-metallic hollow cylinder with a step joint are analyzed. These models combine the effect of notch and material discontinuities as well as those of radial vibration. Large stress gradients in the ragion of the joint cause significant bending of the threaded flanges.

TABLE OF CONTENTS

iv

LIST OF FIGURES

CHAPTER 1

INTRODUCTION

The work presented in this report is a study of stress wave propagation in a bi-metallic, jointed, hollow cylinder subjected to suddenly applied axial loads. This study initiates basic research for evaluating structural integrity of certain ballistic components subjected to severe transient loads. The goal is to develop a technology base of a class of ballistic components formed by joining two cylindrical structures.

Time-varying loads are often classified either as quasi-static or dynamic according to the time elapsed from initiation of loading to attainment of peak load (rise time). Under quasi-static loading, forces are applied slowly relative to the time required for a stress wave to traverse the structure. Typically, these loads reach their peak monotonically in a few milliseconds or more. Dynamic loads are applied more rapidly. Some early electromagnetic gus, for example, impart a force on a projectile which peaks in 35 microseconds.

One of the consequences of dynamic loading is the generation of stress waves which can effect structural integrity. In thread jointed structures, for example, joint failures have been attributed to stress waves which have been amplified locally by reflection at free surfaces or material interfaces and have been disturbed by partial interface gaps.

In this investigation, a finite element model of a 16-inch long hollow cylinder made of half aluminum and half steel, joined mid-length, is subjected to a 60,000 psi stress pulse lasting 16 microseconds and stress wave response is evaluated. The stress wave travels axially from the aluminum base and is followed as it traverses the structure. The effects of structural and material discontinuities at the joint are evaluated.

In this report a review of the fundamental concepts of stress wave propagation is provided in the appendix as reference for the reader. The effect of stress waves meeting a plane boundary between two semi-infinite half spaces of dissimilar material as analytically determined by Kolsky and enhanced by Rinehart and others, is presented.

1

Chapter 2 discusses the ANSYS finite element program used to analyze the various model configurations. Criteria are established which determine the element type and dimensions, time step size, and type of analysis. A substantial portion of the problem solving process consists of determining modelling procedures which result in both accurate and efficient computations. Pitfalls encountered by using simplified modelling techniques are discussed.

In Chapter 3 the results of several analyses are presented and used to discuss the effects of stress waves on various structural configurations. Initially, very simple geometries subjected to stress waves are evaluated for the purpose of proving the finite element techniques. Next, the proven techniques are used to study stress wave propagation in increasingly complex geometries.

Chapter 4 provides a summary of the conclusions resulting from this study.

CHAPTER 2

DYNAMIC FINITE ELEMENT APPROACH

The finite element analysis was performed using the ANSYS finite element program on an Apollo mini-computer network. The ANSYS finite element program is capable of modelling a dynamic event such as that studied in the present case. Swanson Analysis Systems, Inc., the owner of the ANSYS code, has developed a set of empirically derived requirements designed to assure an accurate modelling of stress waves. Experience has shown that poor modelling techniques result in false stress or strain predictions and the analyst may either underestimate the stresses or be overly conservative. Specifications relating to element size, number of elements, and the time step size are provided based on benchmark tests on a bar with two-node elements. Results of the finite element calculations were compared with accepted analytical predictions.

The criteria for an acceptably accurate model requires a maximum element size of L/20 and a maximum time step of L/(60c) whereL is the length of the structure or stress-pulse length, whichever is shorter, and c is the wave speed. If more elements are used, and the integration time step is made smaller, greater accuracy will result. There is a practical limit to the accuracy attainable. Halving the time step or element size will not necessarily double the accuracy but it is certain to at least double the run time. After a certain point, which depends on computer size and speed, increases in accuracy will not be noticeable and computer charges will escalate.

The ANSYS code provides two types of dynamic analyses. The first is the reduced transient analysis in which certain techniques are employed to reduce the number of computations. The second is very general. In the reduced analysis, the time step size is made constant. This saves computations since the nodal velocity and acceleration at each time depend only on the time step duration and not on displacements at prior times. Also, the system degrees of freedom are reduced by concentrating the mass at "master" nodes (Guyan reduction). The penalty for this convenience is some loss of possible mode shapes of structural vibration since the number of mode shapes is directly related to the number of degrees of freedom. Thus, some loss of accuracy can be expected. However, for very uncomplicated structures where the mass is uniformly distributed and no discontinuites exist, the reduced

3

analysis will provide sufficient accuracy and convergence will occur more quickly than by the non-reduced analysis.

The reduced analysis was first attempted for the analysis of the joined cylinders in the interest of economy of time and cost. The essential degrees of freedom, or master nodes, to which mass points were assigned, were identified by inspection. However, oscillatory motion (200,000 Hertz) between master nodes was evident in the displacement response. The addition of more master nodes reduced this effect but the solutions accordingly took longer to converge. Eventually, it was determined that the number of master nodes required for acceptably small levels of oscillation would exceed the allowable number specified by the code. The full, non-reduced version which does not use the matrix reduction technique was therefore adopted for the analyses. It was subsequently found that the difference between convergence times of the full and reduced analyses was insignificant.

Having established the type of analysis, it is then necessary to determine the type of element, maximum element size and time step. A solid rod, for which the response could be accurately predicted was chosen for this purpose. After satisfactory results were obtained, more complex geometries could then be analyzed with a high level of confidence.

After appropriate values of element size and time step were determined, many configurations of rods and hollow cylinders were analyzed. The type of element employed is a 2-D quadrilateral isoparametric with parabolic displacement shape capability on the sides. A model length of 16 inches was chosen for all configurations. This length permits a sufficient number of reflections to be seen without the data exceeding the storage capacity of the computer. The element size was determined to be 0.16 inch in the direction of wave travel, and the time step was calculated to be 0.25 microsecond.

The modelling techniques were further tested on relatively simple discontinuities, such as a notch and a plane interface between two metals. By examining the effects of each dicontinuity separately, a model combining all of them is more easily understood. The first several sections of Chapter 3 discuss these discontinuity models.

CHAPTER 3

EFFECT OF STRESS WAVES ON VARIOUS CONFIGURATIONS

In this chapter the propagation of stress waves in several configurations of rods and hollow cylinders is explored.

A finite element analysis of the stress and displacement response of a straight solid rod with a material discontinuity is first carried out and compared to the well-known analytical solution.

A sequence of hollow cylinders is then analyzed, increasing in complexity from a homogenous cylinder to a bi-metallic cylinder with a step joint and gap elements. A progression of analyses is necessary since radial vibration modes, excited by the forcing function, interact with the stress waves in the cylinder.

3.1 Stress Waves in a Bi-metallic Rod

The finite element grid of a one-inch diameter, by 16-inch long bi-metallic rod made of aluminum and steel is shown in Figure 3.1.1. A symmetric triangular transient stress pulse with a 60,000 psi peak value and duration of 16 microseconds is applied to the base of the rod. The pulse length, calculated by multiplying the wave speed (200,000 inches per second) by the duration, is approximately 3.2 inches. With this pulse length, a dynamic event is established since it is much shorter than the model length.

Using the analysis presented in the appendix, The predicted stress level in the rod will increase by 146 percent as the wave crosses the interface from the aluminum into the steel. A compressive wave at 46 percent of the stress level of the incident wave is reflected back.

Figure 3.1.2 illustrates the stress histories of four elements at various distances along the rod. The red curve is the stress history of element 20 near the bottom. The green curve is for element 80 just below the interface. The blue curve is for element 120 above of the interface and the stress history of element 180, near the top, is depicted by the magenta curve. Examination of the green and blue curves (elements 80 and 120) show the expected

5

1 16" BIMET BAR, PLANE-JOINT, 16 MUSEC R-0-R-0 200 ELEMENTS

Figure 3.1.1. Finite Element Grid of the Bi-metallic Bar

VALU
(1E+5)

1.00 ─
 .80 ─
 .60 ─
 .40 ─
 .20 ─
   0 ─
-.20 ─
-.40 ─
-.60 ─
-.80 ─
-1.00 ─

0   .20   .40   .60   .80   1.00   1.20   1.40   1.60   1.80   2.00   TIME
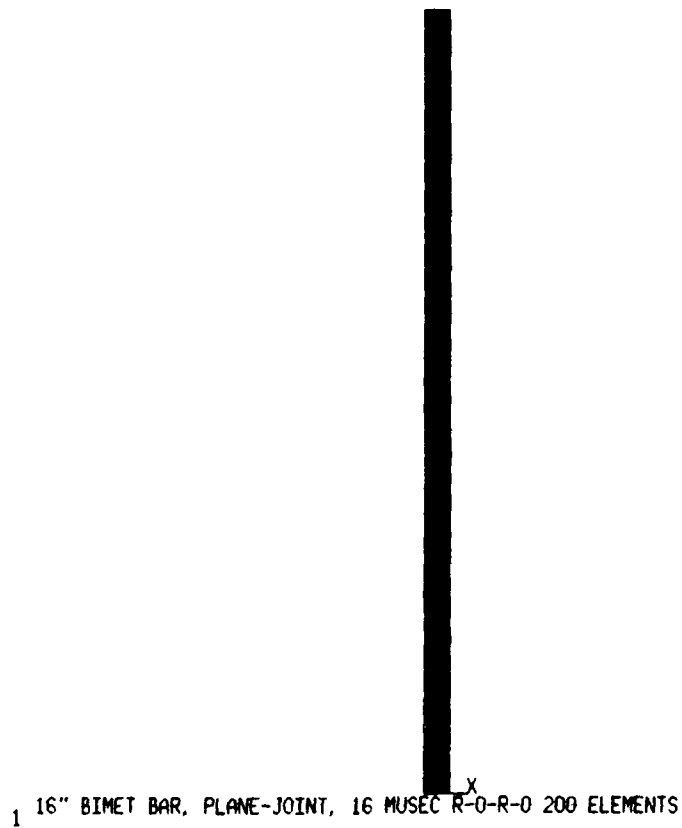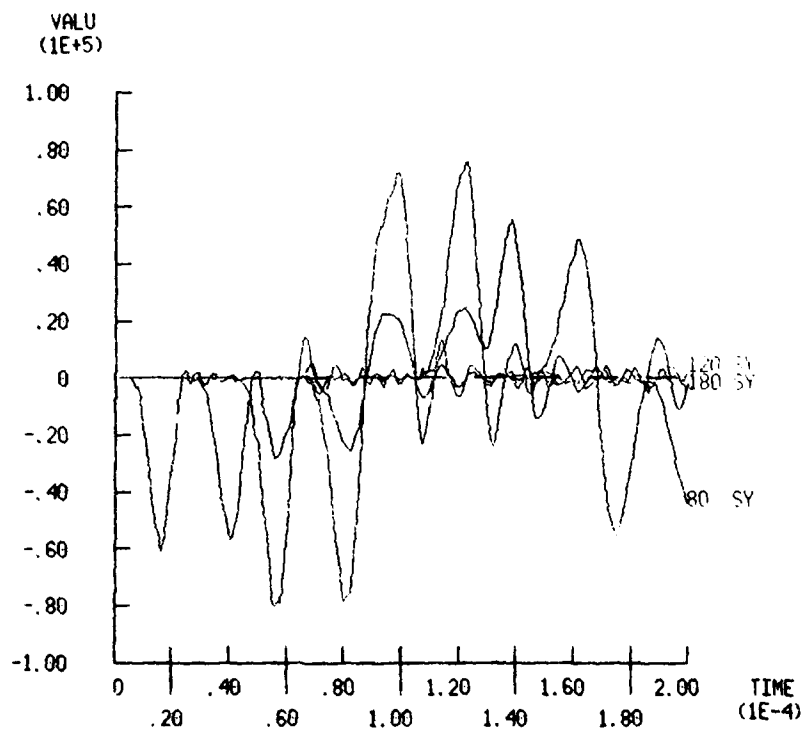   (1E-4)

16" BIMET BAR, PLANE-JOINT, 16 MUSEC R-O-R-O 200 ELEMENTS

Figure 3.1.2. Stress Histories of Key Elements in the Bar

7

increase in stress level across the boundary to be very near the prediction of 146 percent. At 60 microseconds element 80 experiences the reflected pulse at a stress level of approximately 46 percent of the incident pulse; in agreement with the prediction. Focusing attention on the magenta curve, element 180, it can be seen that the compression wave meets the free surface of the end of the rod at about 90 microseconds and reflects as a tensile wave of the same magnitude.

This examination of the response of the bi-metallic rod shows that the wave speed and magnitude of the stress waves are in close agreement with the predictions of the analytical solutions.

3.2 Effect of Stress Wave Propagation on a Hollow Homogenous Cylinder

The same stress pulse as was applied to the solid rod was next applied to a hollow aluminum cylinder, shown in Figure 3.2.1. Element response histories are shown in Figure 3.2.2 where the red curve is the stress history of element 40, which is near the base, and the blue curve is element 160 near the top. The initial pass of the pulse through elements 40 and 160 can be seen at approximately 20 and 70 microseconds respectively. The loss in amplitude is attributed to the energy transfer to strain in the hoop direction. This effect cannot be seen on the solid bar.

The stress pulse reflections from the top end of the cylinder are obscured by the onset of radial vibration which significantly interacts with the axial stress patterns. The radial vibration is seen in Figure 3.2.3, which shows a plot of the radial displacement of a corner node of element 40. The frequency of this mode of vibration can be determined by measuring the period. The period is found to be 60 microseconds which gives a frequency of 16,666 Hertz.

A frequency spectrum plot of the motion of the node is shown in Figure 3.2.4. The dominant mode of vibration is very near that calculated above. Thus, it might be concluded that the 16,666 Hertz mode is excited by the 16 microsecond pulse.

The effect of pulse duration on radial vibration response is further explored in Figure 3.2.5 which illustrates the radial motion of the same node as in Figure 3.2.3. Here the hollow cylinder is subjected to a 256
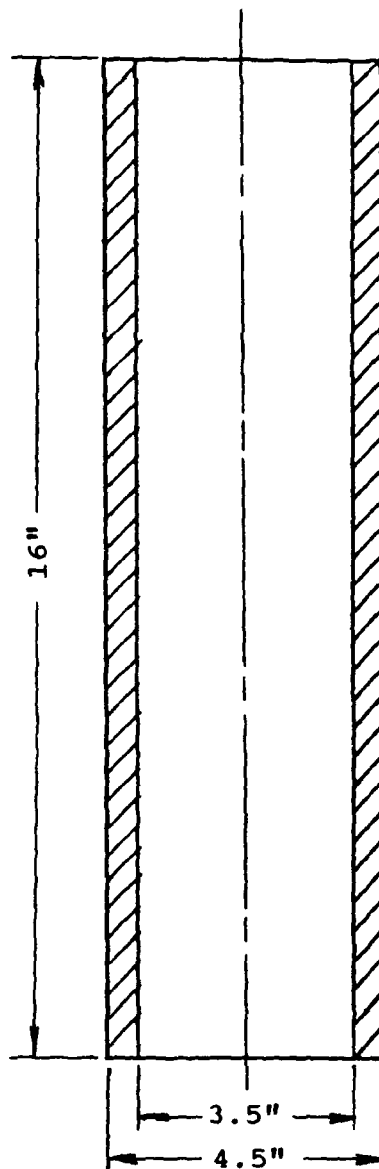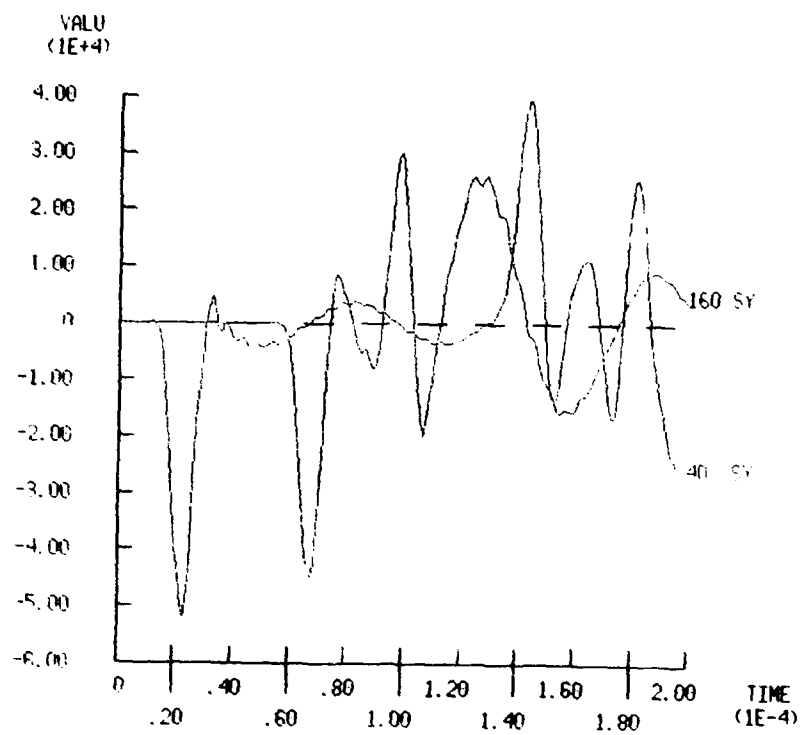
8

Figure 3.2.1. Hollow Aluminum Cylinder

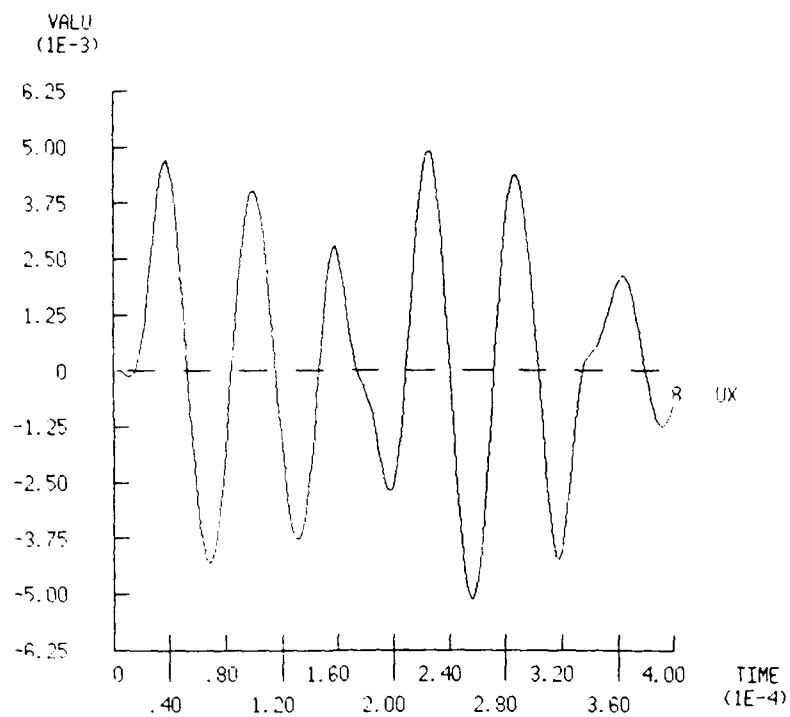Figure 3.2.2. Stress Histories of Key Elements in the
Hollow Cylinder

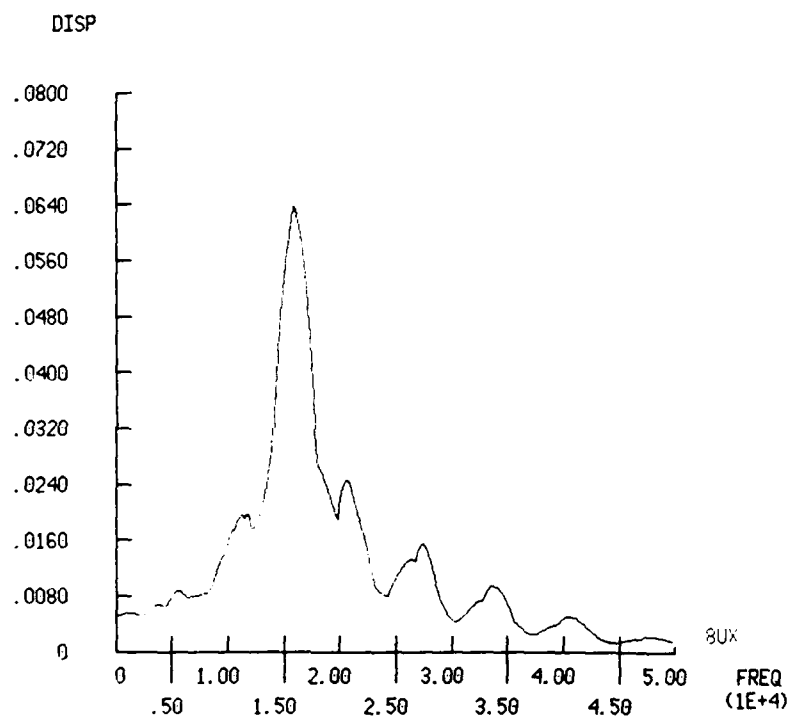Figure 3.2.3. Radial Displacement History of Node #8

Figure 3.2.4. Frequency Spectrum Plot of the Radial
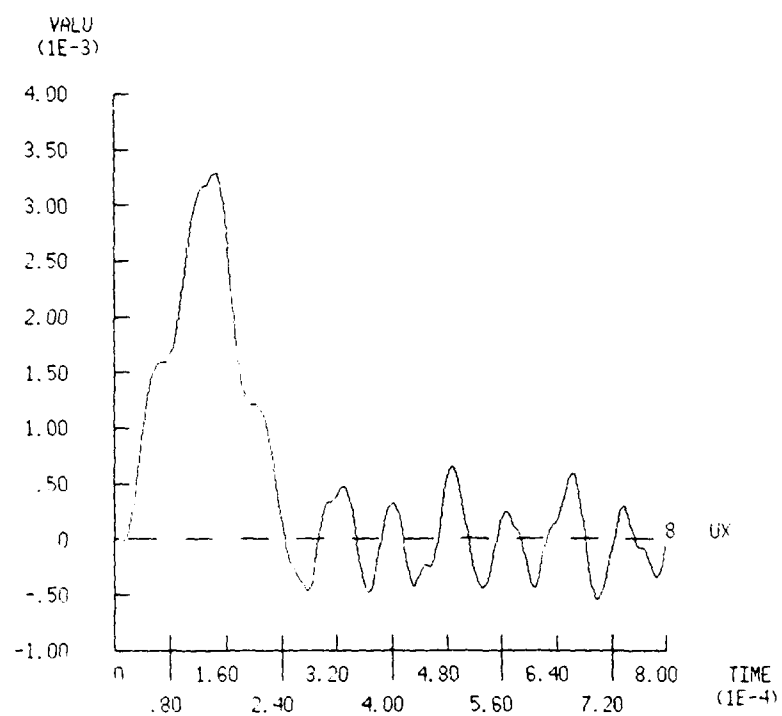Displacement History of Node #8

Figure 3.2.5. Displacement History of Node #8 Resulting
From Long Stress Pulse

13

microsecond duration pulse with a 60,000 psi peak value. The frequency spectrum plot, shown in Figure 3.2.6, shows that the prominent frequency is approximately 12,000 Hertz which is much lower than that excited by the earlier 16 microsecond pulse.

A modal analysis using ANSYS was performed to further explore the effects of radial vibrations. There are, of course, many possible mode shapes associated with this cylinder. Three of these mode shapes with frequencies near 16,000 Hertz are plotted in Figures 3.2.7 through 3.2.9. It can be seen how the bending of the cylinder wall contributes to the overall stress state.

The axial stress resulting from the applied pulse also oscillates back and forth between the ends of the cylinder. The pulse takes about 80 microseconds to travel the length of the cylinder so a complete cycle takes 160 microseconds. Inverting this period yields a frequency of 6250 hertz. The stress pulse, cycling back and forth between the ends of the cylinder, passes through any given point on the cylinder at regular intervals. Since that point on the cylinder wall is also undergoing oscillatory radial motion at a higher frequency there is no regularity or uniformity to the stress patterns.

Although the radial vibration phenomenon is only explored for the homogenous cylinder, all of the hollow cylinder configurations have similar vibration effects and the axial stress patterns are likewise disturbed.

3.3 Effect of Applied Pulse Duration on a Hollow Cylinder

It is appropriate next to investigate the effect of pulse duration on the stress response of a hollow cylinder to demonstrate the difference between dynamic and quasi-static loading which was mentioned in the introduction. If the pulse becomes long relative to the length of the structure, many of the reflections at interfaces or free surfaces tend to fold over on themselves thereby reducing the peak stresses. At a free surface, for example, the incident compression wave can be partially or mostly cancelled by the reflected tensile wave.

The hollow homogenous cylinder was subjected to pulse loads of 16, 32, 64, and 256 microseconds duration. These produced pulse lengths of 3.2, 6.4, 12.8. and 51.2 inches respectively. Figures 3.3.1 through 3.3.4 depict the stress response at points of the cylinder to these loads. As in

14
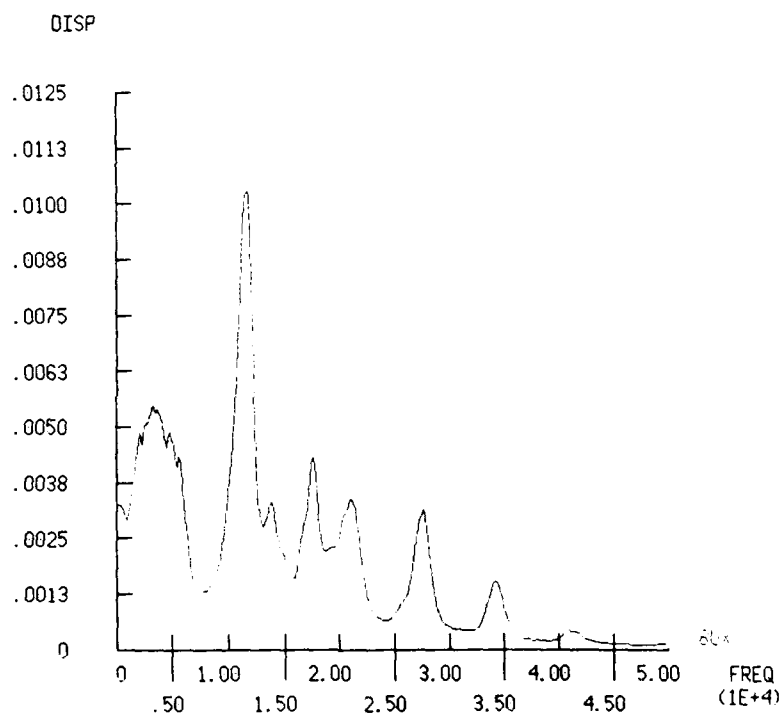
Figure 3.2.6. Frequency Spectrum Plot of the Displacement
of Node #8 Resulting From Long Stress Pulse

16" SOLID-CYLINDER MODAL ANALYSIS 100 ELMTS 10 SHAPES
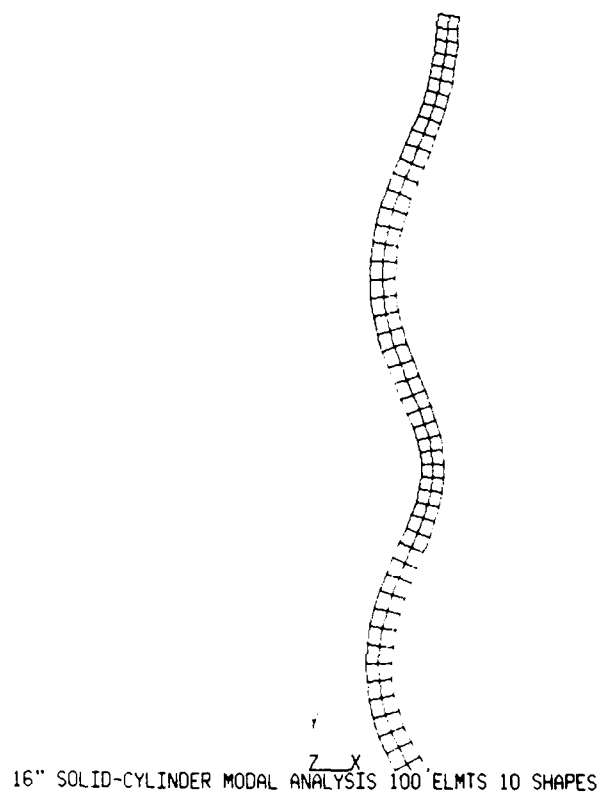
Figure 3.2.7. Mode Shape at 15,712 Hertz.
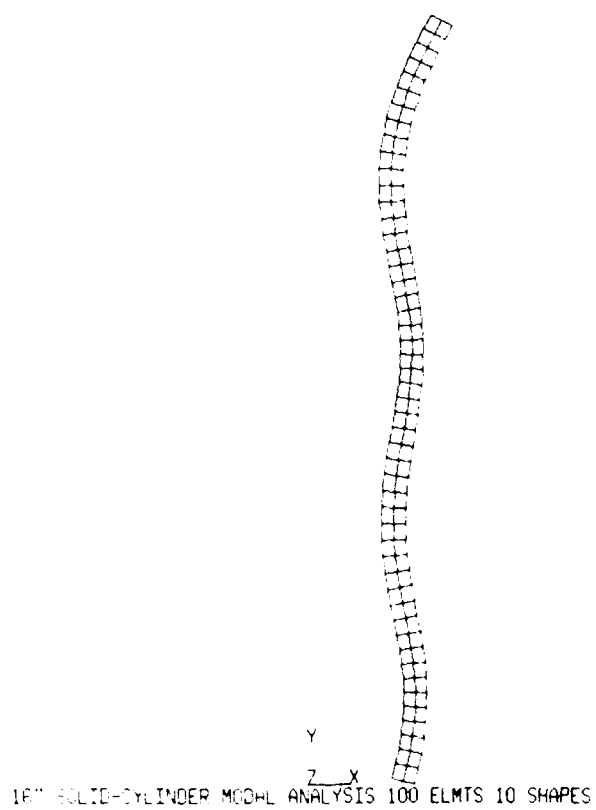
Figure 3.2.8. Mode Shape at 15,975 Hertz.

17

16" SOLID-CYLINDER MODAL ANALYSIS 100 ELMTS 10 SHAPES
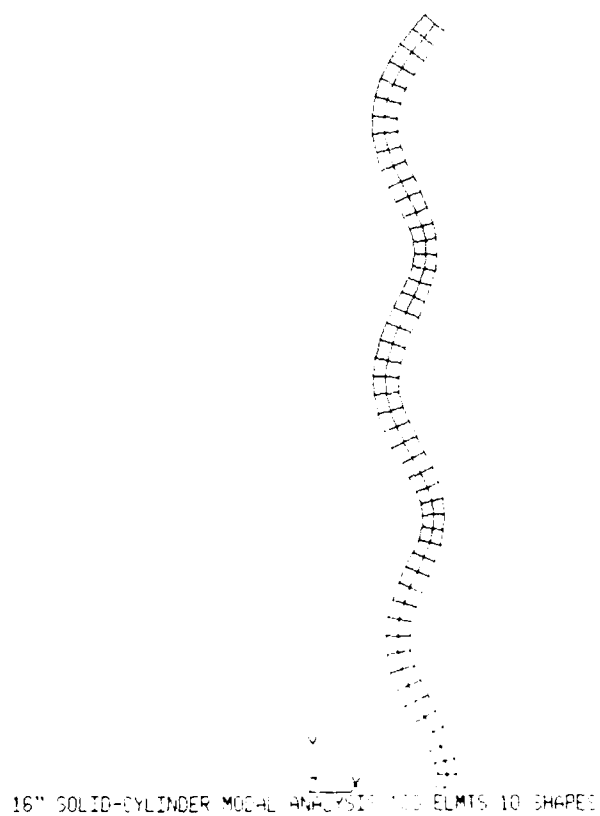
Figure 3.2.9. Mode Shape at 16,350 Hertz.

VALU
(1E+4)
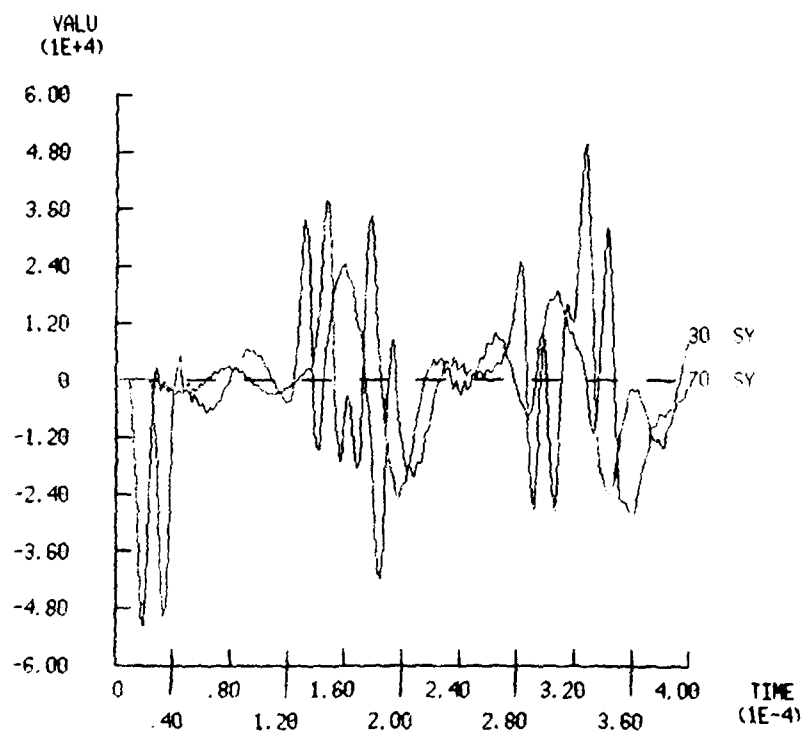
16" SOLID CYLINDER 16 MUSEC RAMPPULSE 200 ELMTS

Figure 3.3.1. Stress Response of Hollow Cylinder to 16
Microsecond Pulse

VALU
(1E+4)

6.00
4.80
3.60
2.40
1.20
0
-1.20
-2.40
-3.60
-4.80
-6.00

30 SY
70 SY

0   .80   1.60   2.40   3.20   4.00   TIME
  .40   1.20   2.00   2.80   3.60   (1E-4)
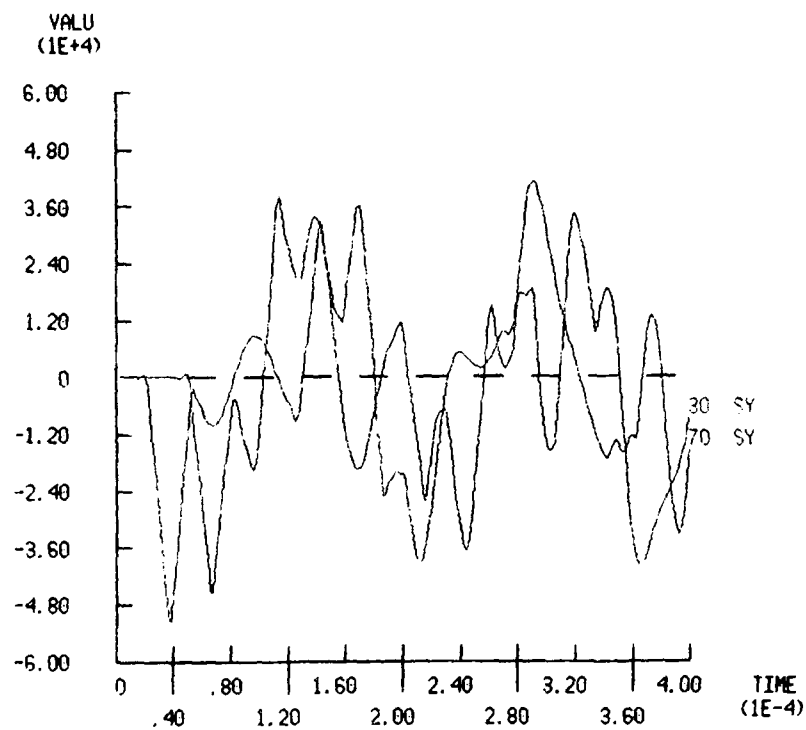
16" SOLID CYLINDER 32 MUSEC RAMPPULSE 100 ELMTS

Figure 3.3.2. Stress Response of Hollow Cylinder to 32
Microsecond Pulse

20

VALU
(1E+4)

6.00
4.80
3.60
2.40
1.20
0
-1.20
-2.40
-3.60
-4.80
-6.00

0   .40   .80   1.20   1.60   2.00   2.40   2.80   3.20   3.60   4.00

70 SY

30 SY

TIME
(1E-4)

1 16" SOLID CYLINDER 64 MUSEC RAMPPULSE 100 ELMTS

Figure 3.3.3. Stress Response of Hollow Cylinder to 64
Microsecond Pulse

21

VALU
(1E+4)

6.00
4.80
3.60
2.40
1.20
0
-1.20
-2.40
-3.60
-4.80
-6.00

0   .80   1.60   2.40   3.20   4.00   4.80   5.60   6.40   7.20   8.00

30 SY
70 SY

TIME
(1E-4)

16" SOLID CYLINDER 256 MUSEC RAMPPULSE 100 ELMTS

Figure 3.3.4. Stress Response of Hollow Cylinder to 256
Microsecond Pulse

22

the previous cases, a symmetric, triangular pulse load with a peak value of 60,000 psi is applied to the base of the cylinder.

Figure 3.3.1 depicts the stress history responses of element 30, near the base, and element 70, near the top of the cylinder to an applied stress pulse of 16 microsecond duration. The onset of vibration is evident immediately after the stress wave passes each element. Several cycles of axial travel occur during the analysis which covers 400 microseconds.

The stress response of the same two elements as above (30 and 70) is shown in Figure 3.3.2 where the pulse duration is increased to 32 microseconds. There is little difference in either the peak stress or the excited mode of vibration between the 16 and 32 microsecond duration pulses. However, as Figure 3.3.3 illustrates, the effects of the waves folding over on themselves is evident in the stress response of the cylinder to a 64 microsecond duration pulse. Finally, a 256 microsecond pulse is applied to the cyl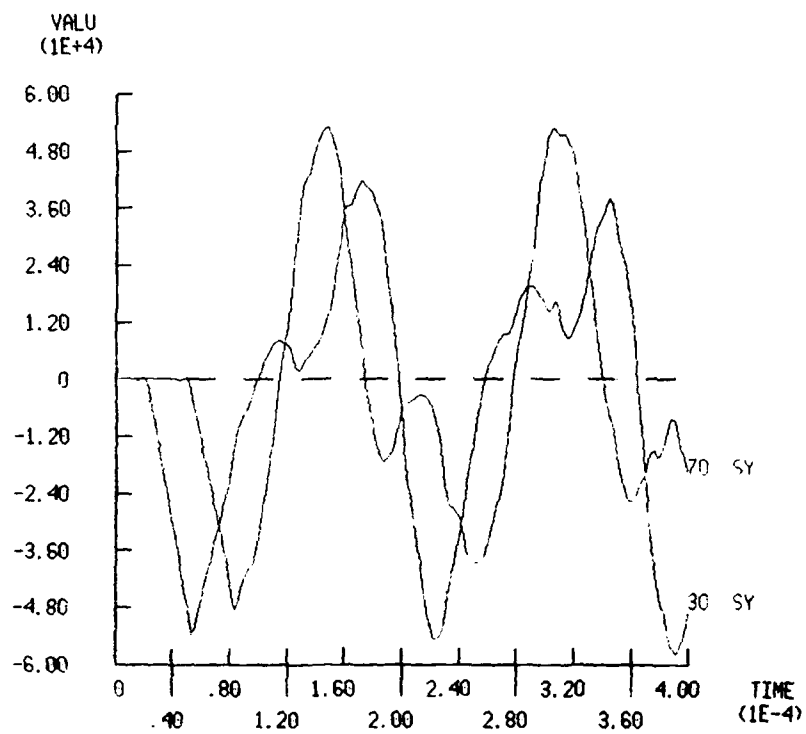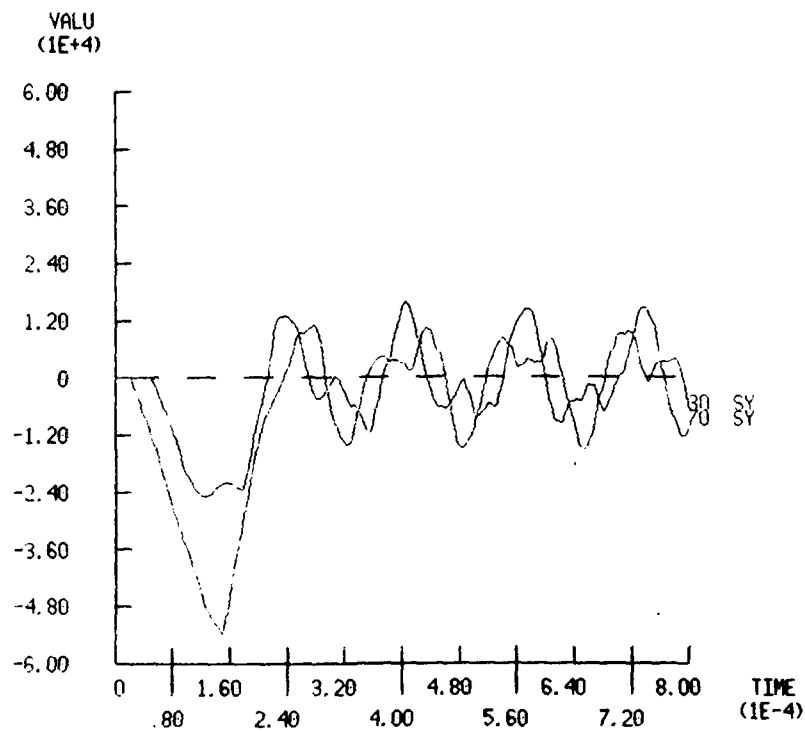inder and the same elements' stress histories are plotted. Figure 3.3.4 shows that only the initial pass of the stress wave is fully developed and that subsequent passes of reflected waves are significantly attenuated.

It might be concluded from this exercise that as the pulse length increases, the effects of stress waves such as reflections and maximum stress, are less pronounced. In the limit, a quasi-static loading case exists for slowly applied loads.

3.4 Effect of Stress Wave Propagation on a Hollow
 Homogenous Cylinder With a Mid-body Square Notch

Thus far, only cylinders with uniform geometries have been examined. Before moving directly to a bi-metallic hollow cylinder with a joint, it is useful to examine a structure whose geometry is intermediate in difficulty between the most simple and most complex cases. This will aid in separating the effects of a notch from those of a bi-metallic interface in the stress histories. Two models are analyzed: a homogenous cylinder with the notch on the inside surface and the other with a notch on the outside surface.

23

3.4.1 Notch on the Inside Surface

Figure 3.4.1 shows the finite element mesh for the hollow cylinder and the location and size of the notch. Also shown are the selected elements whose stress histories will be plotted. The applied load is, again, a 16 microsecond symmetric triangular pulse with a 60,000 psi peak.

When the wave meets the notch, one would expect a partial reflection from the free surface opposite the notch on the inner portion of the cylinder, while the rest of the wave travels on. Figure 3.4.2 is a plot of the stress histories of all the elements through the thickness at a point near the base. The 60,000 psi incident wave passes at 20 microseconds. The wave's magnitude has reduced to about 53,000 psi due to energy transfer to the radial and hoop direction vibration. Later, at 65 microseconds, the expected reflection off the notch can be seen as a tensile wave with a magnitude of about 26 percent of the incident wave. Figure 3.4.3 is a plot of the stress histories of the elements beside the notch through which the wave must travel to reach the upper half. Their average stress is approximately 80,000 psi. This is the portion of the stress wave transmitted through the 46 percent reduced area. This indicates that the amplitude of the transmitted stress wave is not directly proportional to the ratio of connected area to notched area, otherwise, the stress wave in the connected region and the reflected stress pulse would have magnitudes near 53,000 psi. This is due to stress concentration effects in the region of reduced area. This permits the transfer of a greater percentage of stress than would be expected by merely partioning the wave according to the ratio of connected area to notched area. By examining the stress in the four elements just above the notch, Figure 3.4.4, it can be seen how the wave begins to spread out across the thickness after travelling through the reduced area. The wave almost totally reforms before it reaches the end of the cylinder, as shown in Figure 3.4.5, which is a plot of the stress histories of the row of elements four inches beyond the notch. The amplitude of the wave at this point is approximately 41,000 psi, or 74 percent of the value of the initial incident wave before it met the notch. The percentage of the energy traversing the discontinuity is referred to as the stress transmission ratio. Thus, 74 percent of the wave energy is transmitted through 54 percent of the original cross sectional area of the notch.

Conservation of energy can be demonstrated by adding the peak value of the stress wave reflected from the notch

24
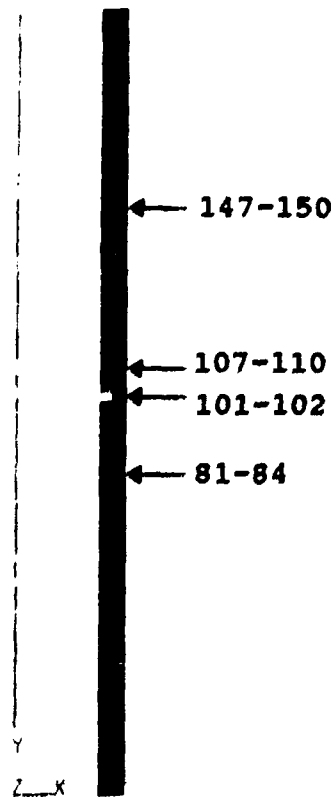
Figure 3.4.1. Finite Element Grid of Inside-Notched Hollow
Cylinder

VALU
(1E+4)

4.00
3.00
2.00
1.00
0
-1.00
-2.00
-3.00
-4.00
-5.00
-6.00

84 SY
83 SY
82 SY
81 SY

0   .20   .40   .60   .80   1.00   1.20   1.40   1.60   1.80   2.00   TIME
(1E-4)
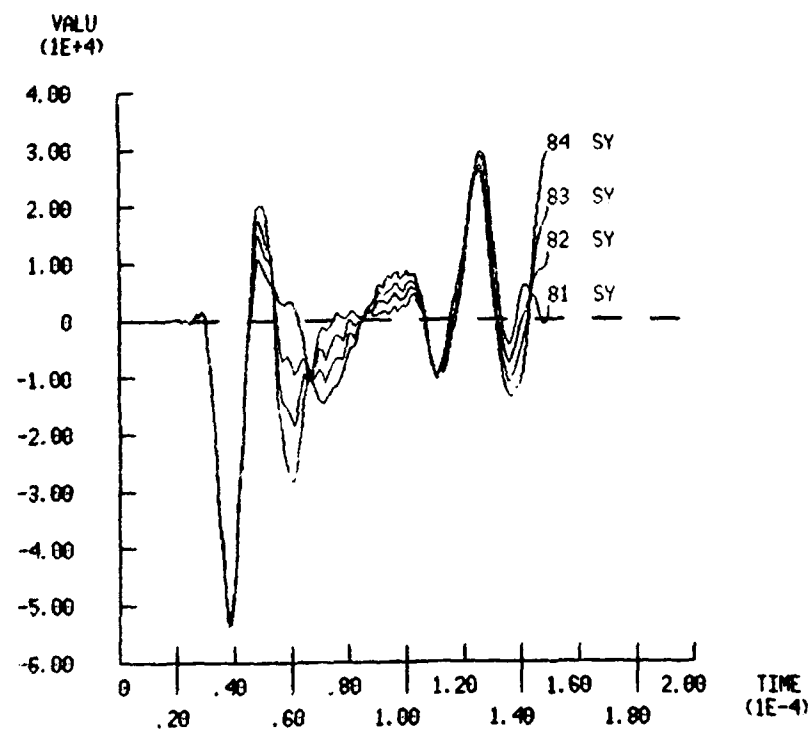
16" SOLID CYL, NOTCHED, 16 MU-SEC PULSE, KAM4

Figure 3.4.2. Stress Histories of a Row of Elements Below
the Notch

26

VALU
(1E+5)
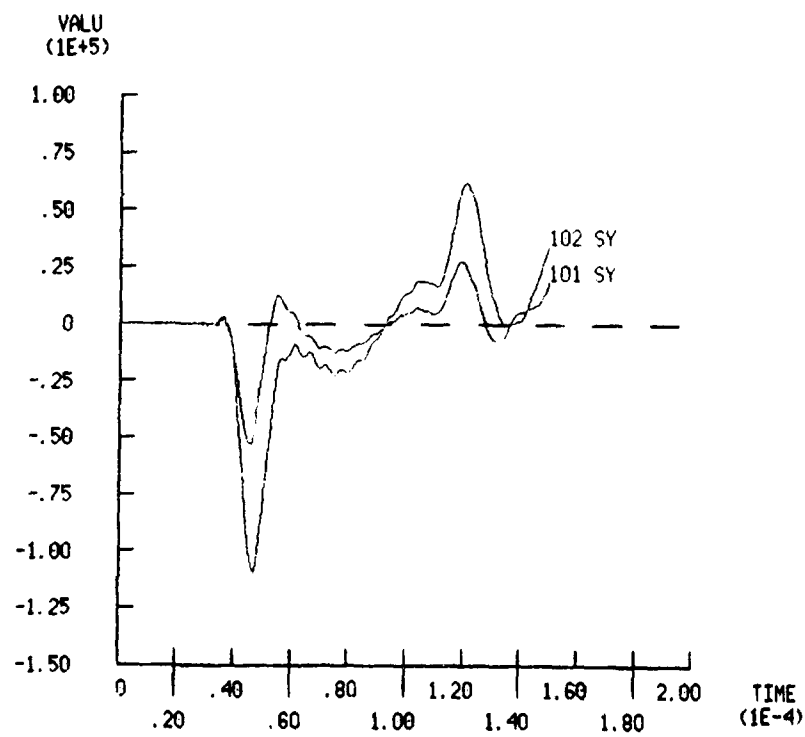
16" SOLID CYL. NOTCHED, 16 MU-SEC PULSE, KAN4

Figure 3.4.3. Stress Histories of the Two Elements Beside
the Notch

27

16" SOLID CYL, NOTCHED, 16 MU-SEC PULSE, KAN4

Figure 3.4.4. Stress Histories of a Row of Elements
Immediately Above the Notch

28

Figure 3.4.5. Stress Histories of a Row of Elements Well
Above the Notch

29

to the peak value of the transmitted wave and comparing to the incident wave's peak stress. Combining the magnitudes of the reflected and transmitted stresses results in nearly the magnitude of the incident wave.

3.4.2 Notch on the Ouside Surface

The effect of reversing the notch location to the outside of the cylinder is next examined. The two stress patterns through the thickness at the same location on the cylinders with inside and outside notches are essentially anti-symmetric as seen in Figure 3.4.6. However, Figure 3.4.7 indicates the stress level is slightly higher through the reduced area on the outside-notched cylinder than on the inside-notched cylinder. This is because the remaining cross-sectional area of the outside-notched cylinder is less than that of the inside-notched cylinder. A calculation of the areas shows that the inside-notched cylinder has 13 percent more connected area at the notch. The stress histories of the elements well above the notch (Figure 3.4.8) indicate an average stress level of 38,000 psi or about seven percent less than the inside-notched cylinder. As found in the previous section, the transmitted stress is not proportional to the remaining wall area.

A further investigation of the non-proportional transmission effect was performed by analyzing an homogenous cylinder with a larger inside notch, reducing the connected region to 27 percent of the cylinder wall thickness (the notch is now 3/8 inches deep on a 1/2 inch wall). The results are illustrated in Figures 3.4.9 and 3.4.10. Figure 3.4.9 shows the incident wave has the same magnitude as that of the two previous cases. The reflected wave from the free surface is greater in magnitude - 26,000 psi (49 percent of the incident wave). The transmitted stress is about 27,000 psi (51 percent of the incident wave) as shown in Figure 3.4.10. Thus, even though the connected cross-sectional area was reduced by 73 percent, 51 percent of the stress was transmitted.

Figure 3.4.11 depicts the transmitted stress relative to notch size for the three notched cylinders. Two additional data points were added based on the assumptions that zero remaining connected area transmits no stress, and 100 percent stress is transmitted for a cylinder without a notch. The remaining connected area, as a percentage of the wall thickness, is plotted on the ordinate and the transmitted stress as a percentage of the incident stress is plotted on the abscissa.

30

VALU
(1E+4)

16" SOLID CYL, NOTCHED, REVERSED, 16 MU-SEC PULSE, KAN4

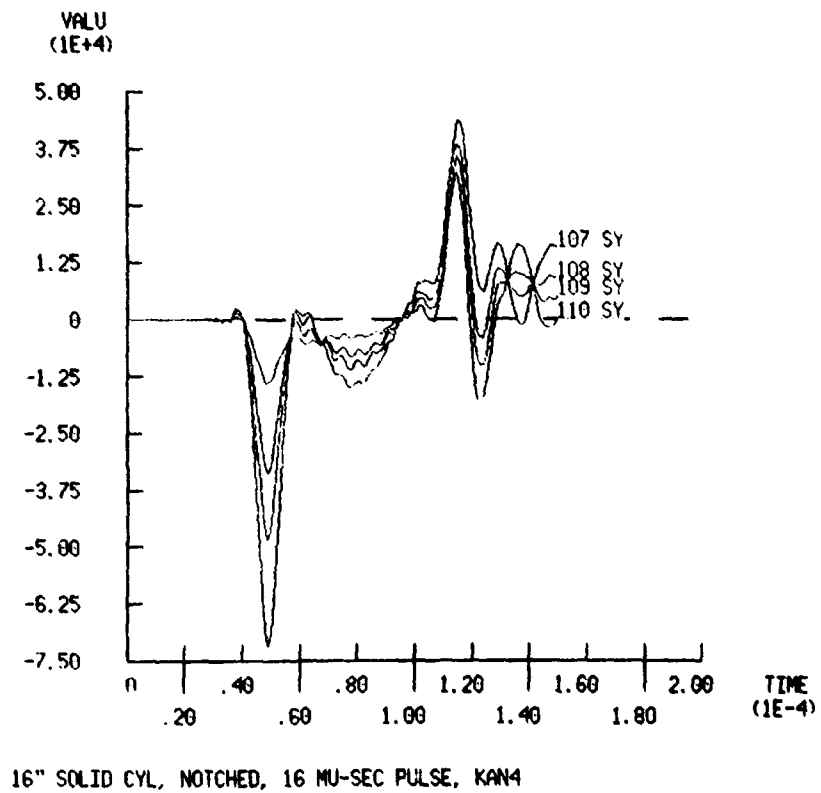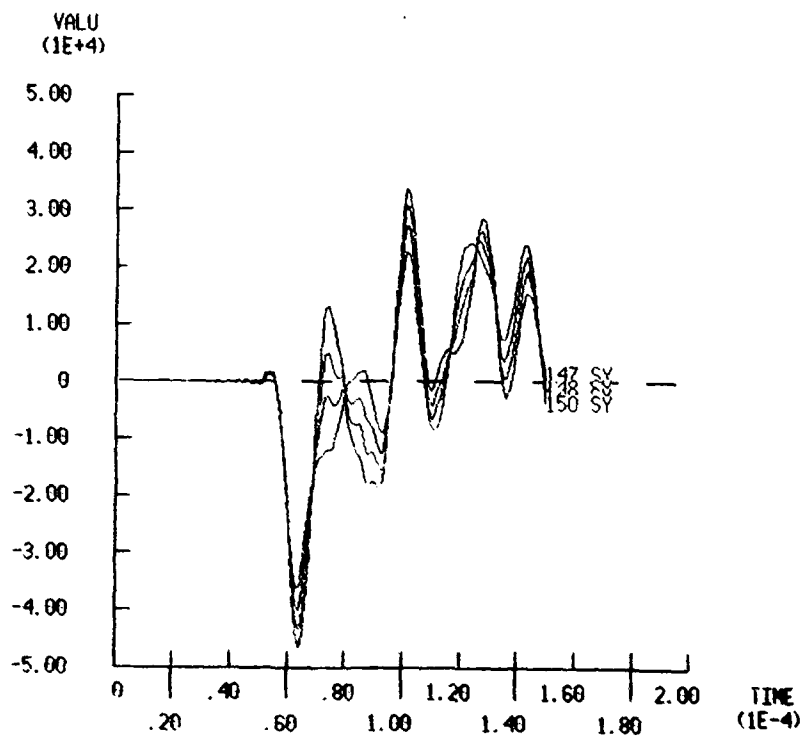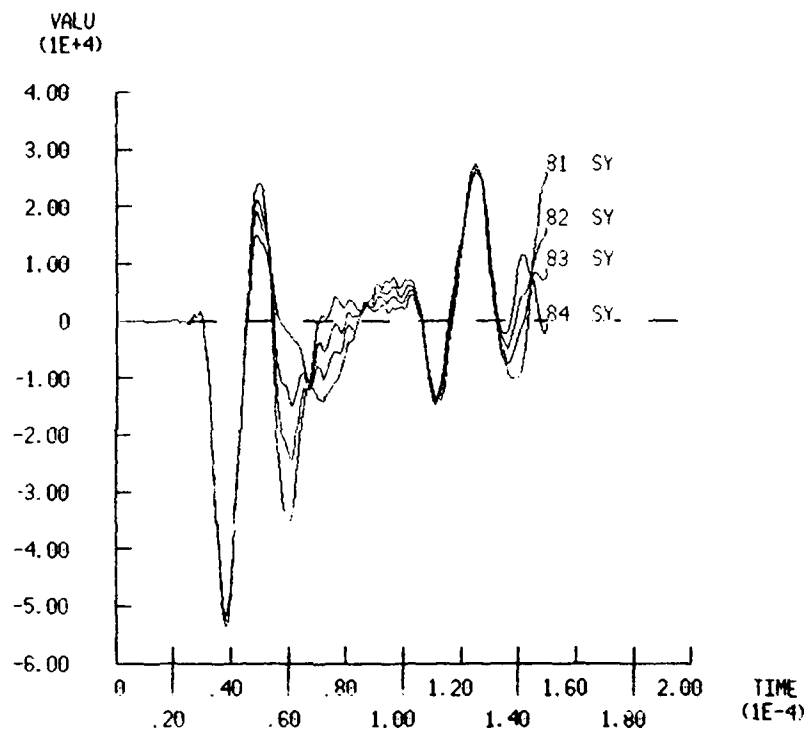Figure 3.4.6. Stress Histories of a Row of Elements Below
the Notch on the Outside-Notched Cylinder

31

VALU
(1E+5)
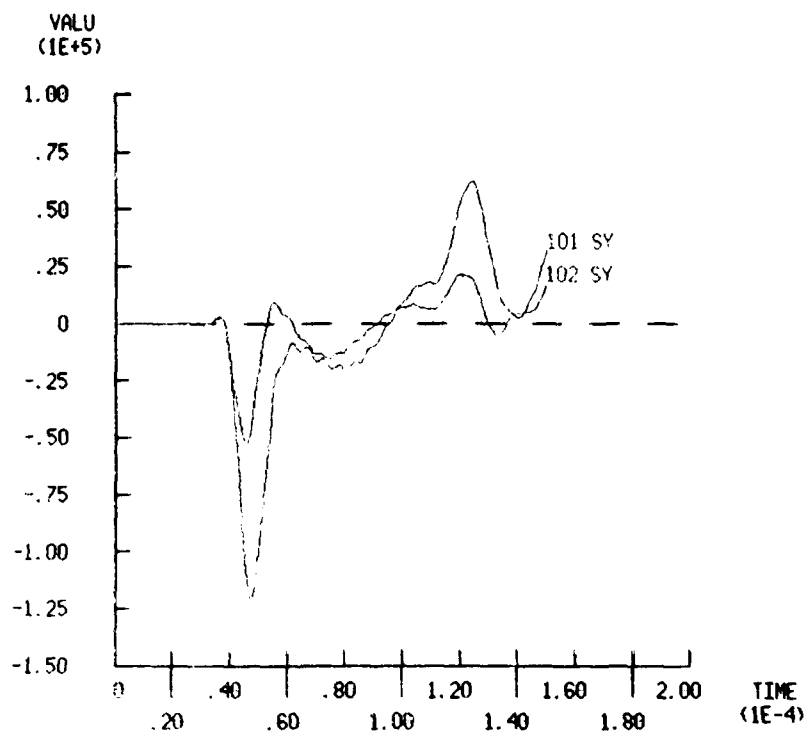
16" SOLID CYL, NOTCHED, REVERSED, 16 MU-SEC PULSE, KAN4

Figure 3.4.7. Stress Histories of the Two Elements Beside
the Notch on the Inside-Notched Cylinder

32

VALU
(1E+4)

5.00
4.00
3.00
2.00
1.00
0
-1.00
-2.00
-3.00
-4.00
-5.00

0   .20   .40   .60   .80   1.00   1.20   1.40   1.60   1.80   2.00   TIME (1E-4)

150 SY
149 SY

16" SOLID CYL, NOTCHED, REVERSED, 16 MU-SEC PULSE, KAN1
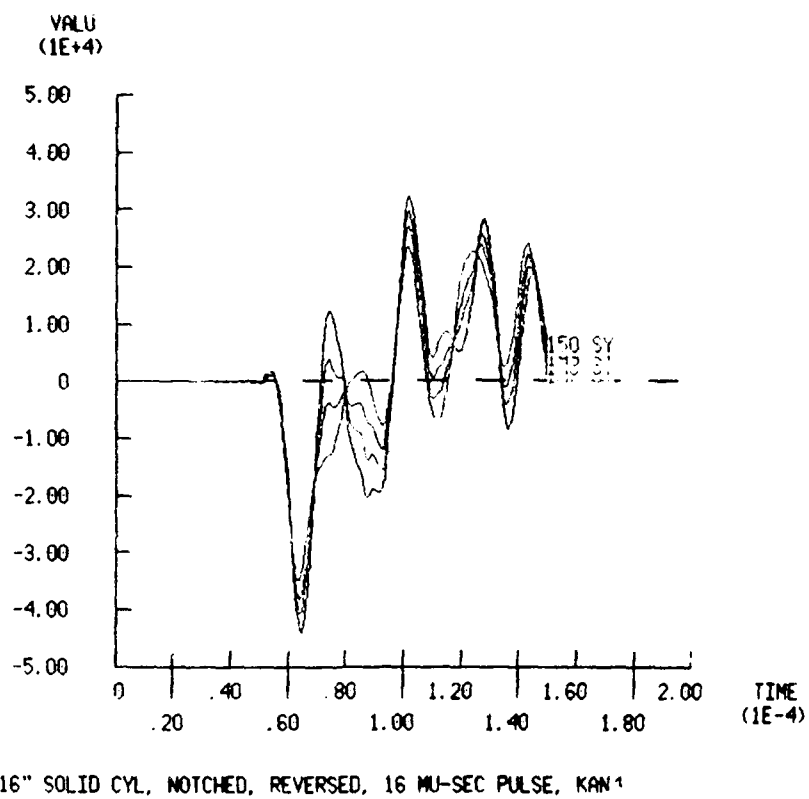
Figure 3.4.8. Stress Histories of a Row of Elements Well Above the Notch on the Inside-Notched Cylinder

33
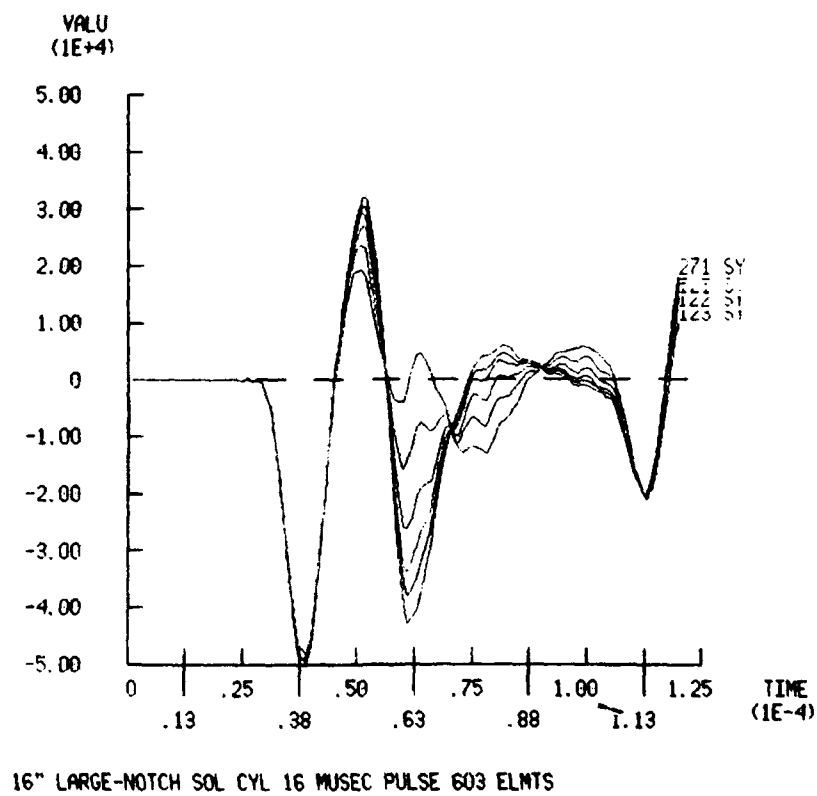
Figure 3.4.9. Stress Histories of a Row of Elements Below
the Notch on the Large-Notched Cylinder

34

VALU
(1E+4)

4.80
4.00
3.20
2.40
1.60
.80
0
-.80
-1.60
-2.40
-3.20

550 SY

0   .25   .50   .75   1.00   1.25   TIME
 .13   .38   .63   .88   1.13   (1E-4)
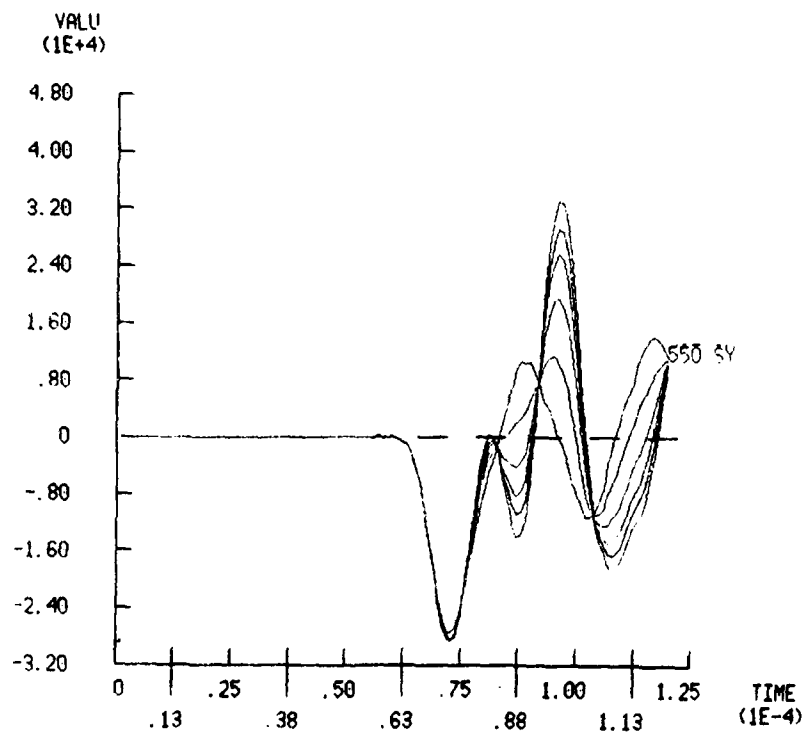
1 16" LARGE-NOTCH SOL CYL 16 MUSEC PULSE 603 ELMTS

Figure 3.4.10. Stress Histories of a Row of Elements Well Above the Notch on the Large-Notched Cylinder
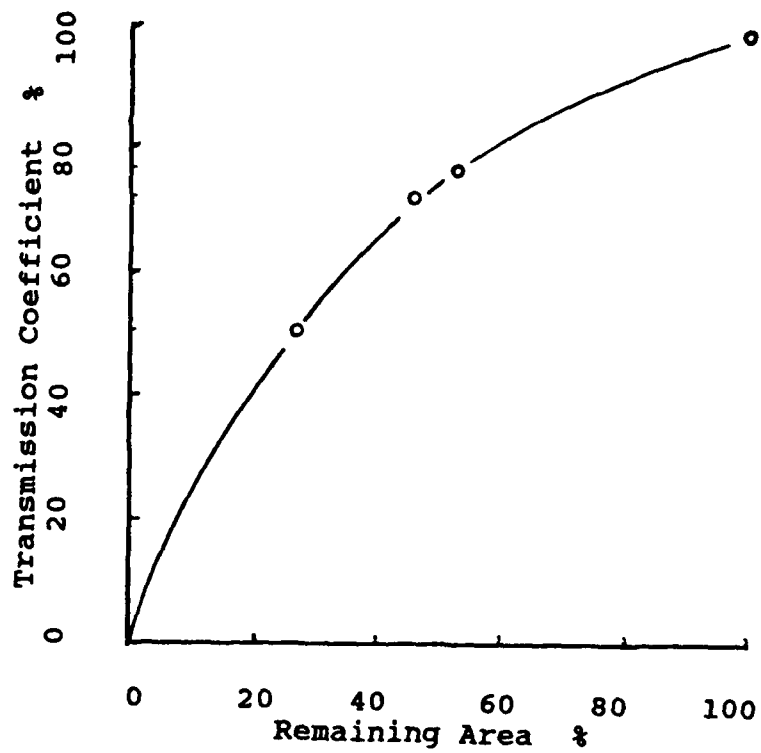
Figure 3.4.11. Transmission Coefficient as a Function of
Remaining Area at the Notch

3.5 Effect of Stress Wave Propagation on a Bi-metallic Hollow Cylinder With a Plane Joint

The propagation of a stress wave through a bi-metallic cylinder with a plane joint is considered before one with a step joint. The stress histories for the elements shown in Figure 3.5.1 are plotted in Figure 3.5.2. These are very similar to the stress histories in the bi-metallic rod in section 3.1 until the onset of vibration after the initial pass of the stress pulse. Careful comparison between Figures 3.1.2 and 3.5.2 reveal a difference in the wave speed manifested by the arrival time of the stress pulse in element 360 for the cylinder, and element 180 in the rod, which are the same axial distance from the base. Hopkins and Chou [3] provide some relationships for wave speed vs geometry. Specifically, the speed of a wave in a bar is slower than that of a sheet of the same material. They do not provide the wave speed for a hollow cylinder, but a hollow cylinder can be thought of as being formed from a sheet wrapped around an axis and thereby has a higher wave speed than a bar. The expressions for wave speed in a bar and sheet are provided below:

$$\text{bar:} \qquad c = (E/p)^{.5} \qquad\qquad (3.5.1)$$

$$\text{sheet:} \qquad c = [E/(1-v^2)p]^{.5} \qquad\qquad (3.5.2)$$

where E is the modulus, p is the density and v is Poisson's ratio.

3.6 Effect of Stress Wave Propagation on a Bi-metallic Cylinder With a Step Joint

Sections 3.1 through 3.5 have provided a foundation for the focus of this investigation: a hollow bi-metallic cylinder with a step joint. The individual effects of a notch, bi-metallic interface, and shell type construction are now combined into one model. The step-jointed bi-metallic cylinder is first evaluated without any displacement continuity across the vertical boundary of this joint between the two cylinders. The pupose of this analysis is to compare stress distributions in the coupled and uncoupled interfaces. The finite element model of the joint is depicted in Figure 3.6.1 where the blue represents aluminum and the red is steel. Then, gap elements are introduced and the two models are compared. In addition, the effect of reversing the joint is evaluated. That is, the male and female components will be interchanged, as illustrated in Figure 3.6.2.

37

Y

Z   X

16" BIMET CYL, PLANE-JOINT, 16 MUSEC R-0-R-0, 400 ELEMENTS

Figure 3.5.1. Finite Element Grid of the Bi-metallic
Cylinder with a Plane Joint

VALU
(1E+5)
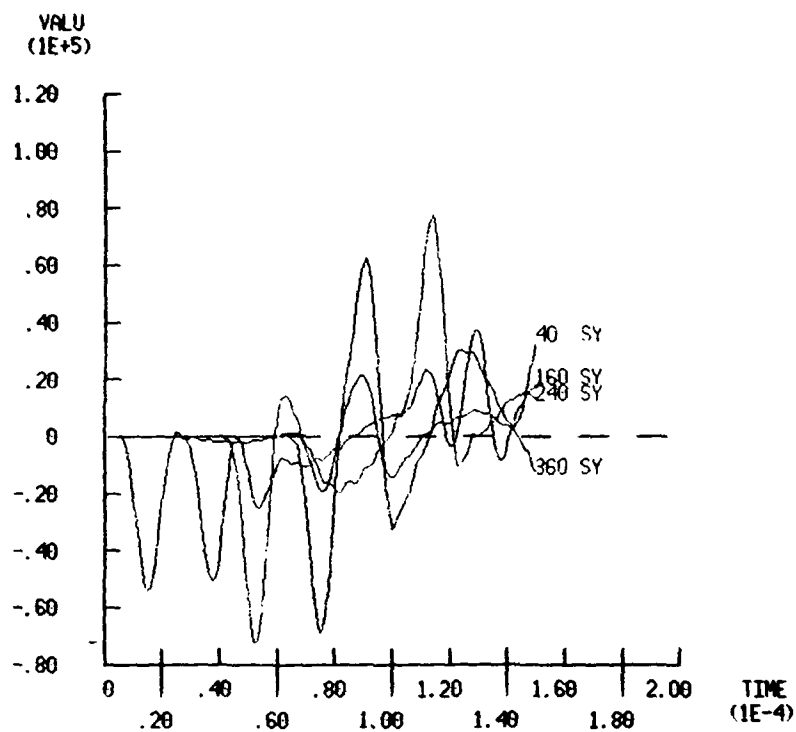
16" BIMET CYL, PLANE-JOINT, 16 MUSEC R-O-R-O, 400 ELEMENTS

Figure 3.5.2. Stress Histories of Key Elements in the
Bi-metallic Cylinder with a Plane Joint
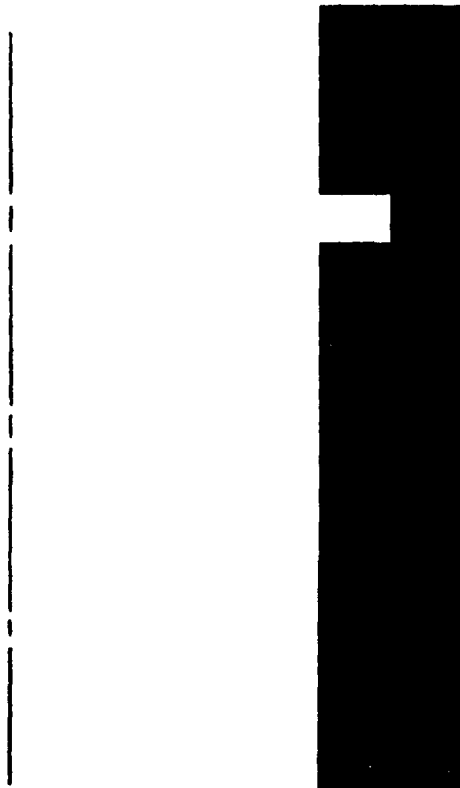
Figure 3.6.1. Finite Element Model of the Step Joint
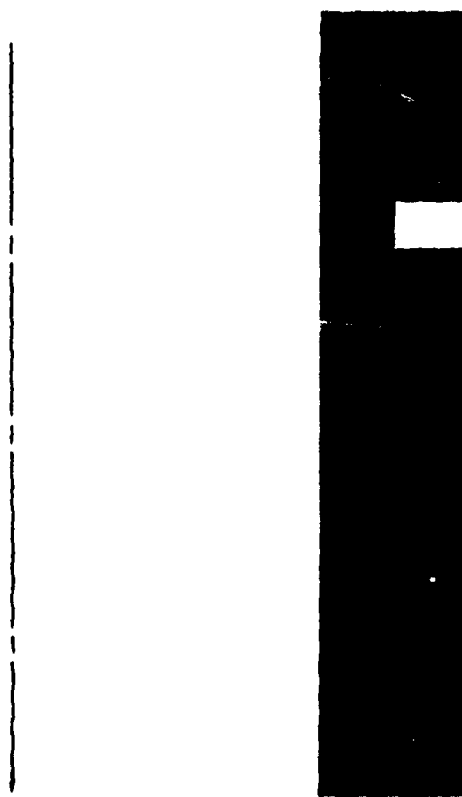
Figure 3.6.2. Finite Element Model of the Reversed Step
Joint

41

3.6.1. Step Joint Without Gap Elements

This model of a bi-metallic hollow cylinder is based on the assumption that no continuity of displacements is maintained between the two cylinders at the steps of the joint (vertical interface where threads may be found). The purpose of this study is to establish a baseline for assessing the contribution of gap elements to joint stress behavior and displacements.

When the stress wave meets the joint shown in Figure 3.6.1, it is partitioned by the vertical interface. The outer portion, which meets the steel flange, reflects some of its energy and transmits the rest. Plane interface theory, presented in the appendix, predicts 146 percent is transmitted and 46 percent is reflected. The other portion of the wave, partitioned toward the inside half of the cylinder wall, travels up the aluminum flange for another 0.75 inch where it meets a free surface. The elapsed time for this portion of the wave to travel the 0.75 inch, reflect, and travel back 0.75 inch is about seven microseconds. This sets up a rather complicated stress pattern in that the reflected tensile wave is now seven microseconds behind a reflected compression wave which is also travelling back toward the base. Figure 3.6.3 illustrates this stress pattern by the stress histories of a row of elements immediately below the joint. At 38 microseconds, the incident wave is seen. Then at 50 microseconds, the reflected tensile wave from the free surface passes back through the elements which has been partially cancelled by the reflected compression wave from the plane portion of the interface where the aluminum meets the steel. Since the inner portion of the cylinder wall is in tension and the outer portion is in compression, some bending is present. An examination of the stress histories of the elements on either side of the vertical interface (elements 116, 117, 124 and 125) between the flanges, shows that the stress transmitted into the steel is greater than the expected 146 percent increase. Figure 3.6.4 shows the stress in the steel flange averages 100,000 psi in compression, nearly twice the value of the incident wave. This is due partly to the change of medium, from aluminum to steel, and partly to the reduction of cross-sectional area of the flange relative to the full wall. An examination of the stresses in the elements further forward (elements 122, 123, 130 and 131 in Figure 3.6.5) shows that the average stress in the steel flange is now 112,000 psi. It is presumed that the stress in the steel elements of Figure 3.6.4 were partially cancelled by the returning tensile wave in adjacent elements (superposition) below the flange. The compressive stresses in the steel flange causes
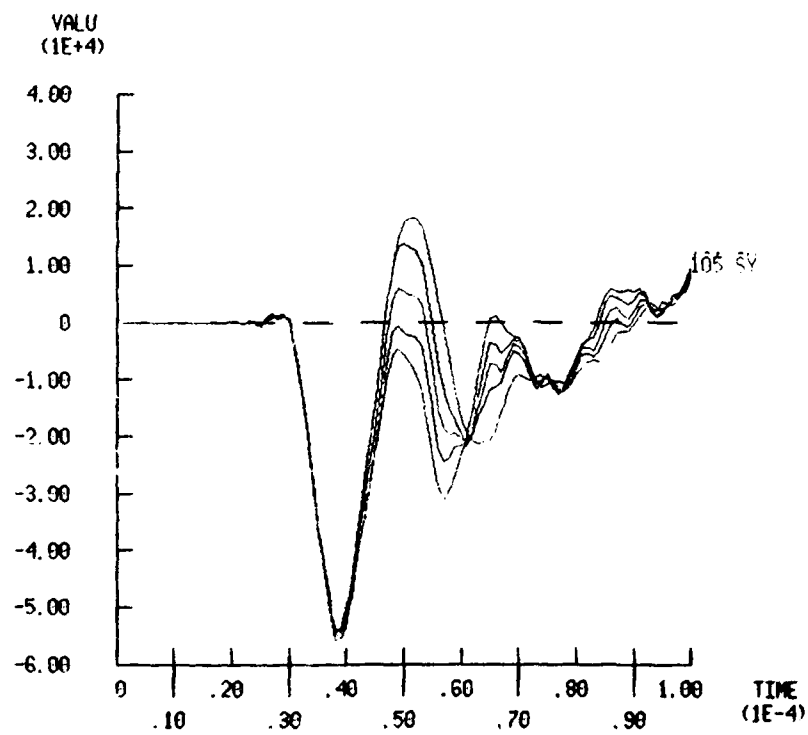
Figure 3.6.3. Stress Histories of the Row of Elements
Immediately Below the Step Joint

43
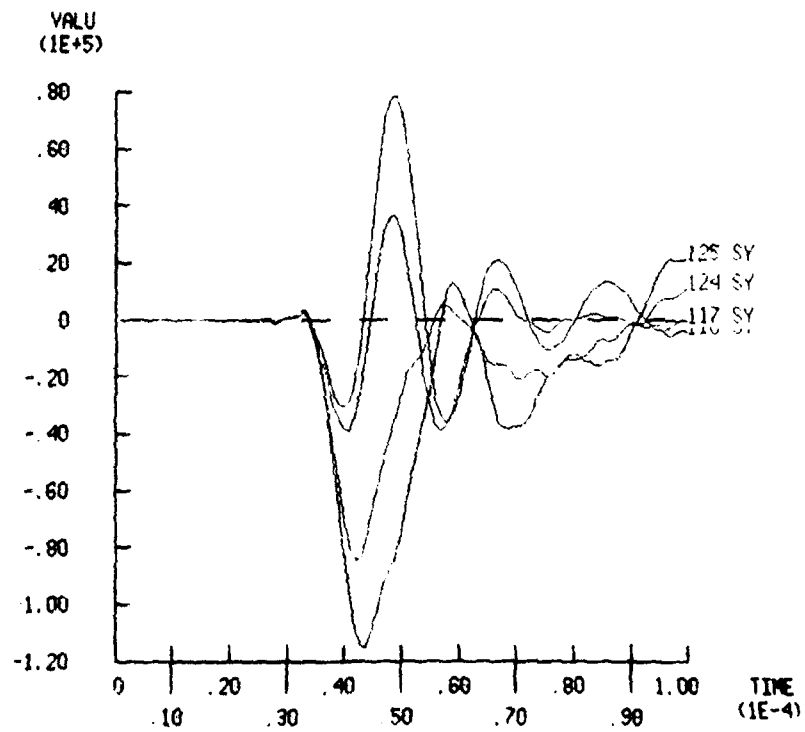
Figure 3.6.4 Stress Histories of the Row of Elements Above the Bottom Step of the Joint

44

VALU
(1E+5)

.80
.60
.40
.20
0
-.20
-.40
-.60
-.80
-1.00
-1.20

131 SY
123 SY

0   .20   .40   .60   .80   1.00   TIME
  .10   .30   .50   .70   .90   (1E-4)

Figure 3.6.5 Stress Histories of a Row of Elements
Immediately Below the Free Surface

45

a barreling effect, as shown in Figure 3.6.6. At the same time, stress gradients in the aluminum flange produce a bending moment, causing it to bend inward toward the axis. Thus, the displacements of the flanges will tend to separate the vertical interface. This separation is quantified in the rext section (3.6.2) where gap elements are utilized.

Figure 3.6.7 depicts the stress histories of a row of elements above the joint. Their average stress level is near 60,000 psi or 113 percent of stress level of the incident wave. Comparison of this transmission coefficient to that for the plane-jointed bi-metallic cylinder, 146 percent, indicates that only 77 percent of the maximum possible stress was transmitted through the step joint. This is consistant with the transmission coefficient for the notched homogeneous cylinder in Section 3.4 whose remaining connected area is equal to that of the step joint model. Thus, even though the transmitted stress is higher for the bi-metallic cylinder, the same percentage of potential stress is transmitted.

3.6.2 Step Joint With Gap Elements

This joint model includes four gap elements at the vertical interface parallel to the axis. Gap elements are used to represent the joint threads since no thread elements are available with the code. It is not practical to model threads with existing elements since the time step required to be compatible with the very small elements necessary to detail a thread would be prohibitively small. Use of gap elements in this region is intended to give information about interface displacements during the passing of a stress wave and the forces transmitted at that time.

The gap element has a Young's modulus of ten million psi in compression and zero in tension. When the interface is in compression, any difference in axial motion between the two nodes of the gap element would result in transmitted force in that direction, similar to a threaded connection. Due to the geometry of the threads it is not possible for axial sliding to occur such as smooth, surfaces would permit. Thus, during radial compression, any shear force would be fully transmitted. The friction coefficient is therefore specified as 1.0.
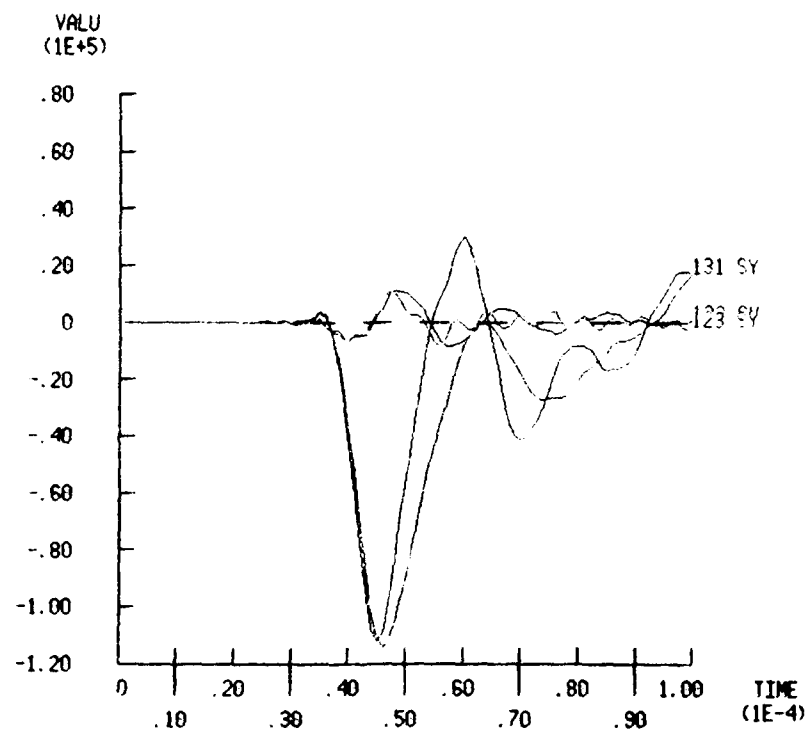
Figure 3.6.8 shows the stress histories of the row of elements below the joint. The stress histories are very

46

```
                                    ANSYS  4.3
                                    JUN  2 1988
                                     9:21:24
                                    POST1 STRESS
                                    STEP=3
                                    ITER=136
                                    TIME=.00005
                                    SY   (AVG)
                                    STRESS GLOBAL

                                    ZV=1
                                    DIST=2.05
                                    XF=2
                                    YF=7.91
                                    MX=81943
                                    MN=-111815
                                        -90000
                                        -65000
                                        -40000
                                        -15000
                                        10000
                                        35000
                                        60000
                                        81943
```
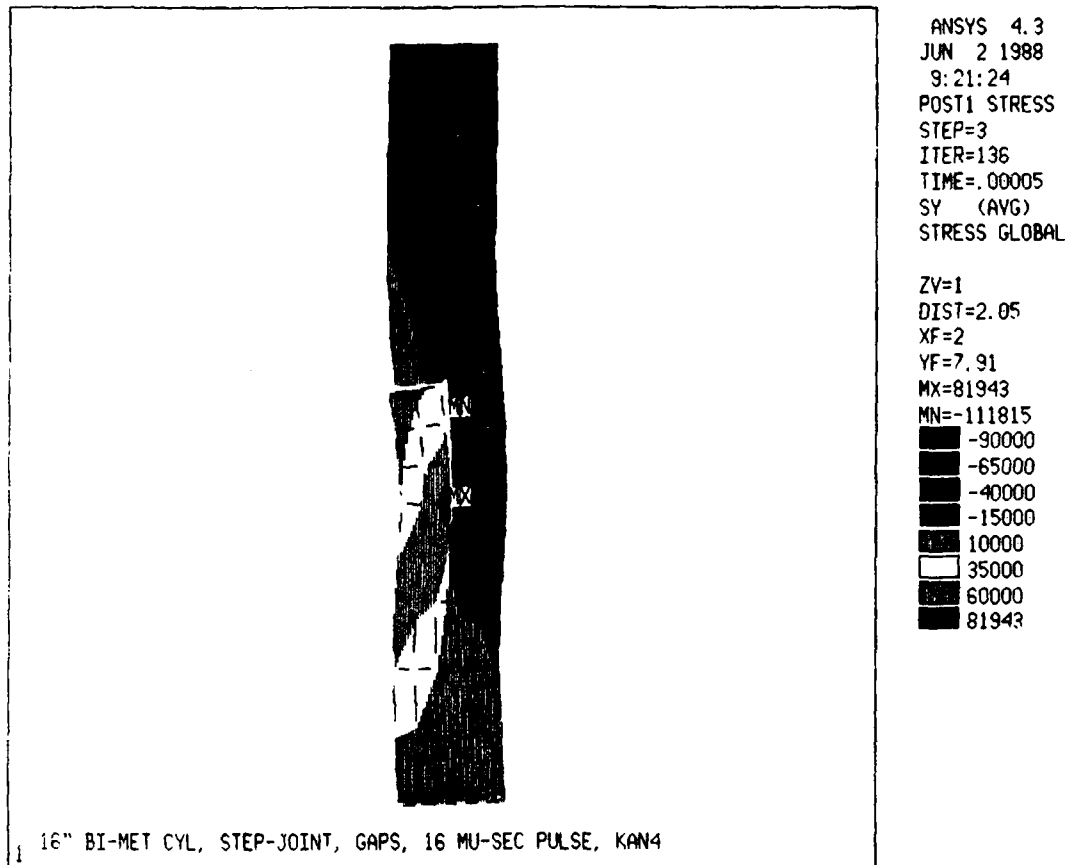
16" BI-MET CYL, STEP-JOINT, GAPS, 16 MU-SEC PULSE, KAN4

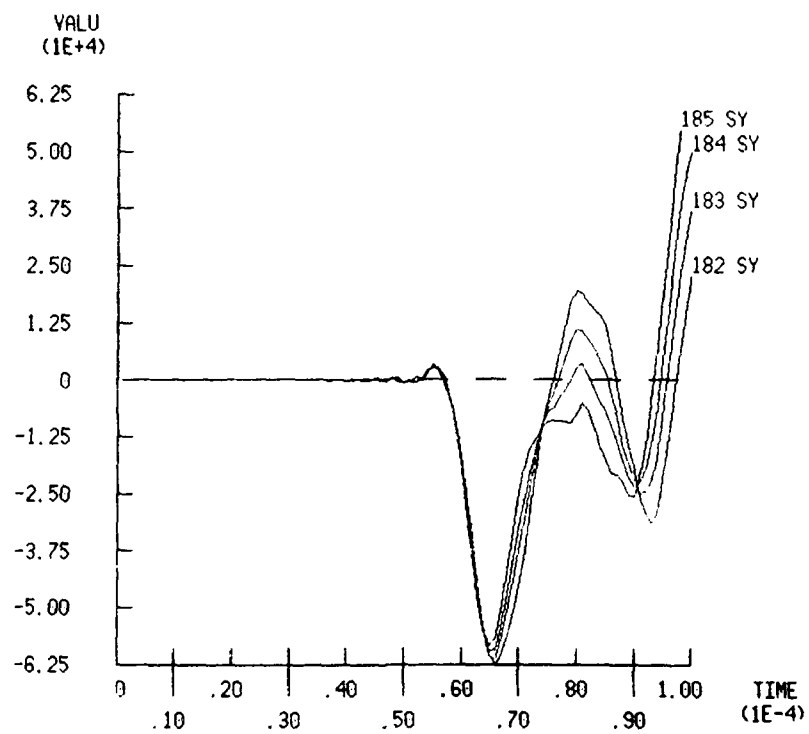Figure 3.6.6. Stress Contours in the Joint Region
at 5) Microseconds

47

Figure 3.6.7. Stress Histories of a Row of Elements Well
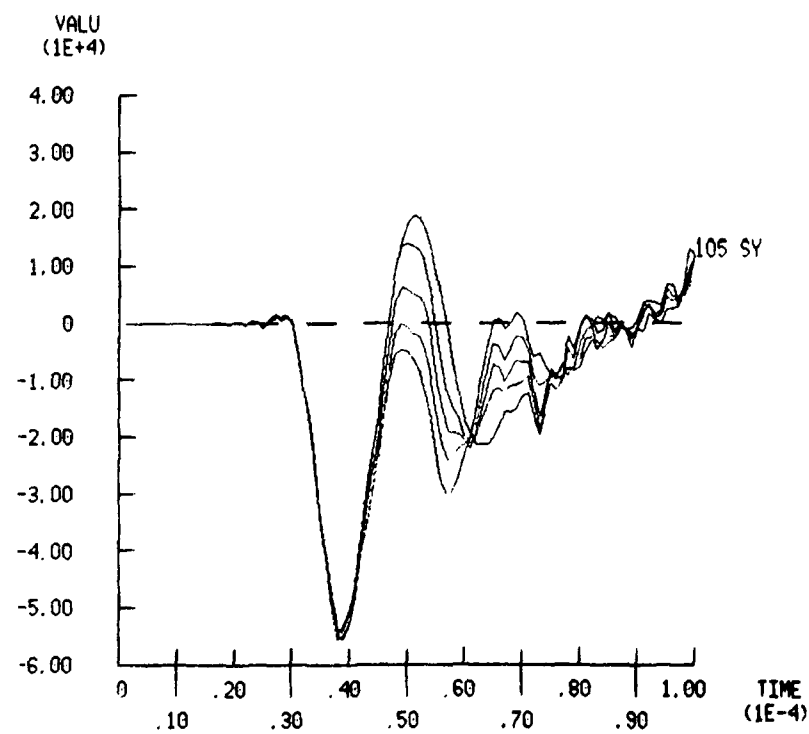Above the Joint

48

VALU
(1E+4)

Figure 3.6.8. Stress Histories of a Row of Elements Below
the Step Joint

49

similar to those in Figure 3.6.3 indicating that the new interface elements have little effect on the overall stress state at this point. Figures 3.6.9 and 3.6.10 are the stress histories of the rows of elements at the bottom and top of the interface region, respectively. There is little difference between these stress histories and those of the same elements in the previous step joint model without gap elements. Similarly, the stress histories of the row of elements well above the joint, Figure 3.6.11, look much like those in Figure 3.6.7 indicating identical transmission coefficients.

Gap behavior is described by Figures 3.6.12 through 3.6.15 which show gap separation, axial sliding, normal force and shear force; all plotted against time.

As Figure 3.6.12 illustrates, the gap is open for most of the duration of the analysis. Closure is indicated by a negative value for clearance. Figure 3.6.13 shows that normal force is transmitted only during gap element compression, indicating that the gap elements are performing as specified. The normal force and the sliding separation of paired nodes making up each gap element (Figure 3.6.14) are the key factors which determine the transmitted shear force shown in Figure 3.6.15. The total shear force transmitted through the joint is determined by adding all the nodal sliding force values. These forces are given in pounds per radian, so it is necessary to multiply by 2*pi to obtain the total force.

The sum of these shear forces is approximately 47,000 pounds. This force, acting on a shear surface which is 9.4 square inches in area, results in a shear stress of approximately 5,000 psi on the interface. The stress in the elements supporting the gap elements, 123 and 130 are only slightly lower than those in the model with an open interface which can be seen by comparing the element stresses in Figures 3.6.5 with those in Figure 3.6.10. This indicates that a small portion of the load is transmitted by the vertical interface (threads in the physical model).

3.6.3 Reversed Step Joint

The effect of reversing the joint examined in section 3.6.2 is next considered. This involves interchanging the male aluminum threads with steel female threads and locating the notch on the outside.
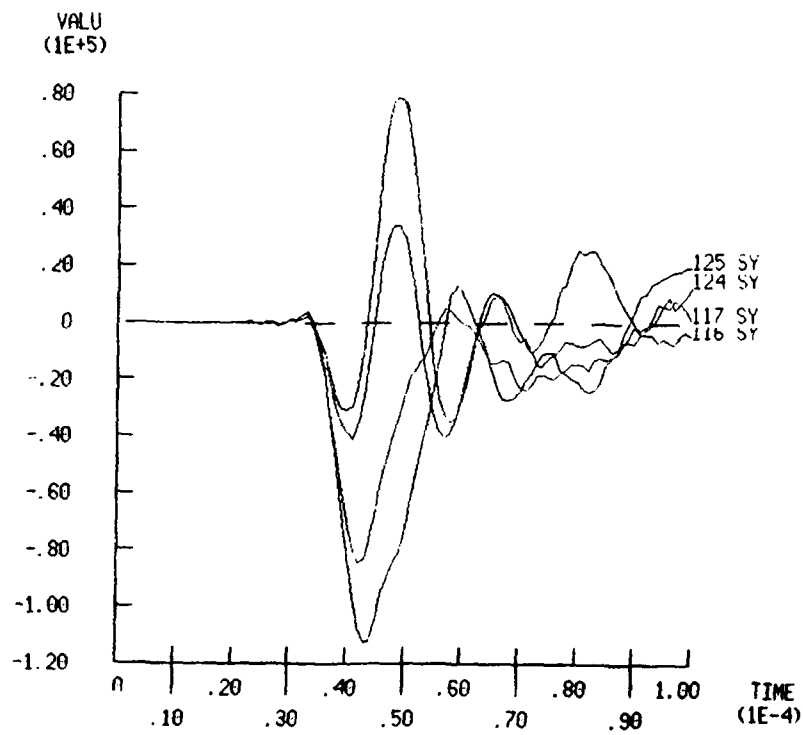
Figure 3.6.9. Stress Histories of the Row of Elements
Above the Bottom of the Step Joint

51
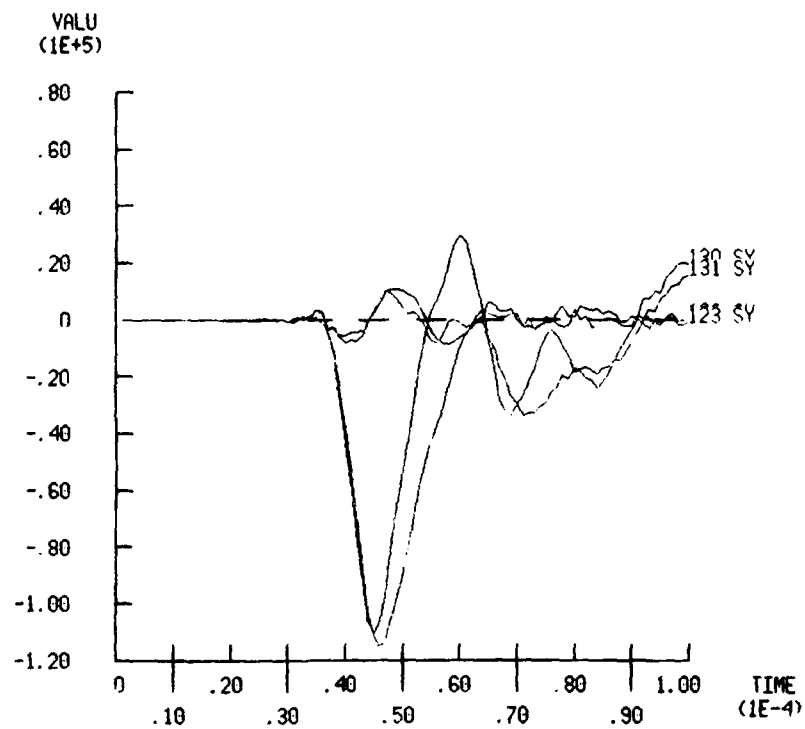
Figure 3.6.10. Stress Histories of the Row of Elements
Immediately Below the Free Surface of
the Step Joint

52
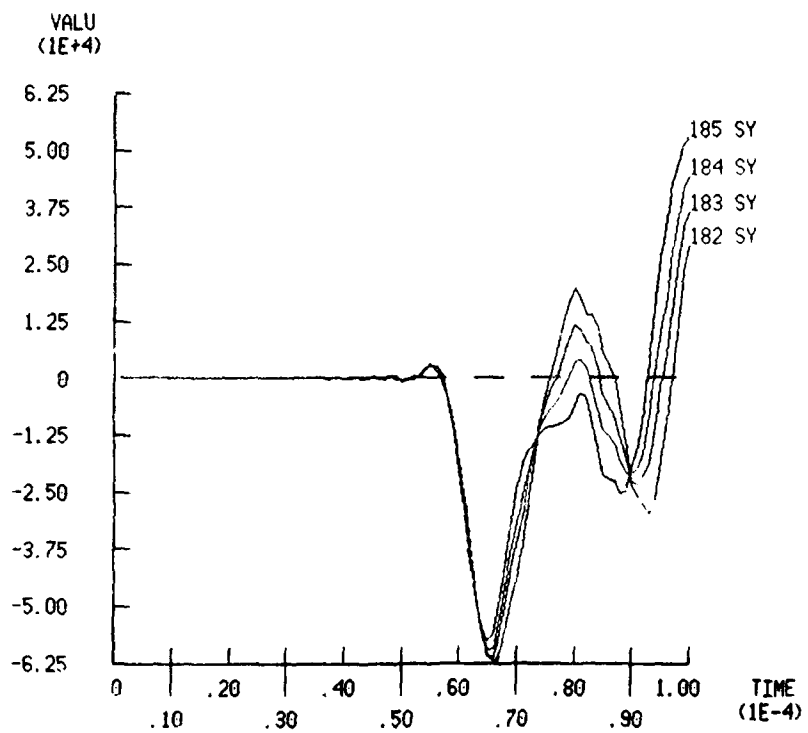
Figure 3.6.11. Stress Histories of a Row of Elements Well
Above the Joint

53
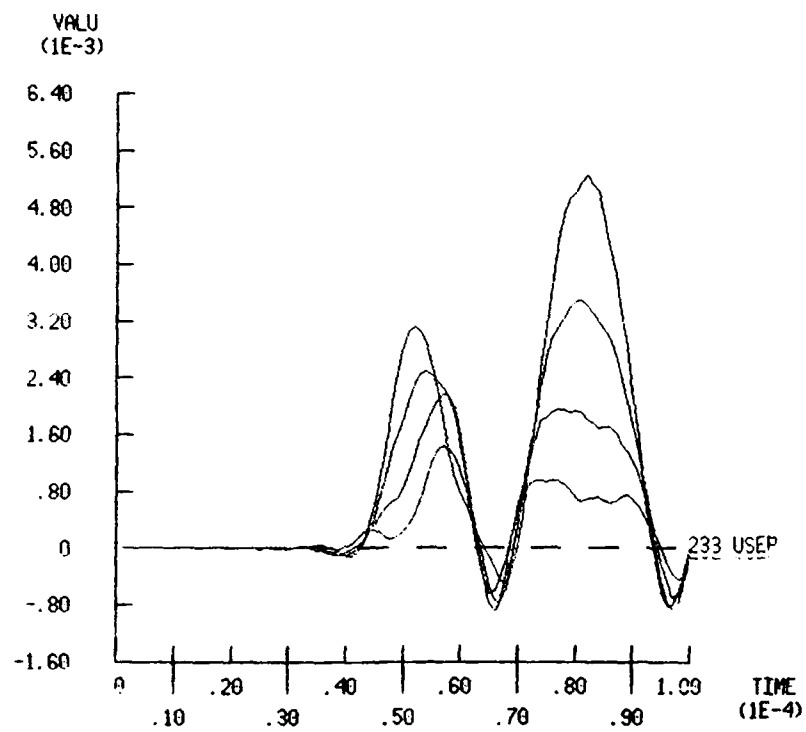
Figure 3.6.12 Gap Element Normal Separation
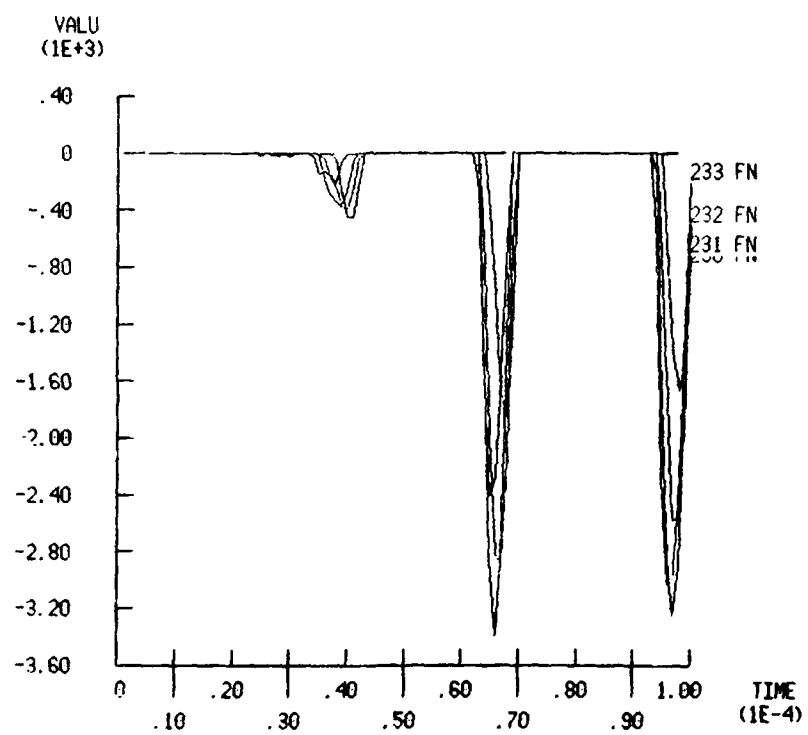
Figure 3.6.13. Gap Element Normal Force

55
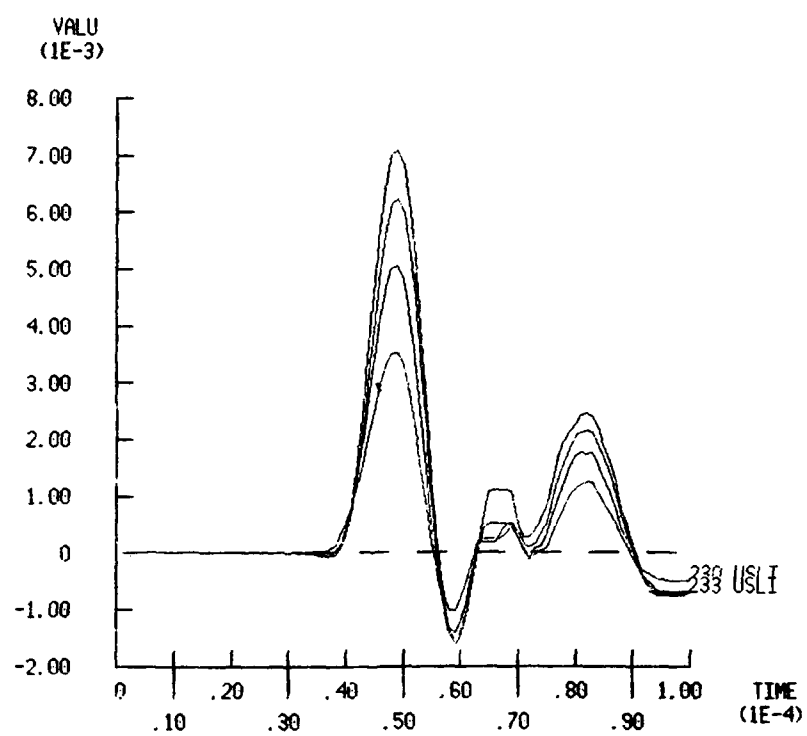
Figure 3.6.14. Gap Element Sliding Separation

56

VALU
(1E+3)

```
 3.00 ┤
 2.50 ┤
 2.00 ┤
 1.50 ┤
 1.00 ┤                                              231 FS
  .50 ┤                                              232 FS
                                                     230 FS
    0 ┤                                              233 FS
 -.50 ┤
-1.00 ┤
-1.50 ┤
-2.00 ┤
      0    .20    .40    .60    .80    1.00   TIME
        .10    .30    .50    .70    .90       (1E-4)
```
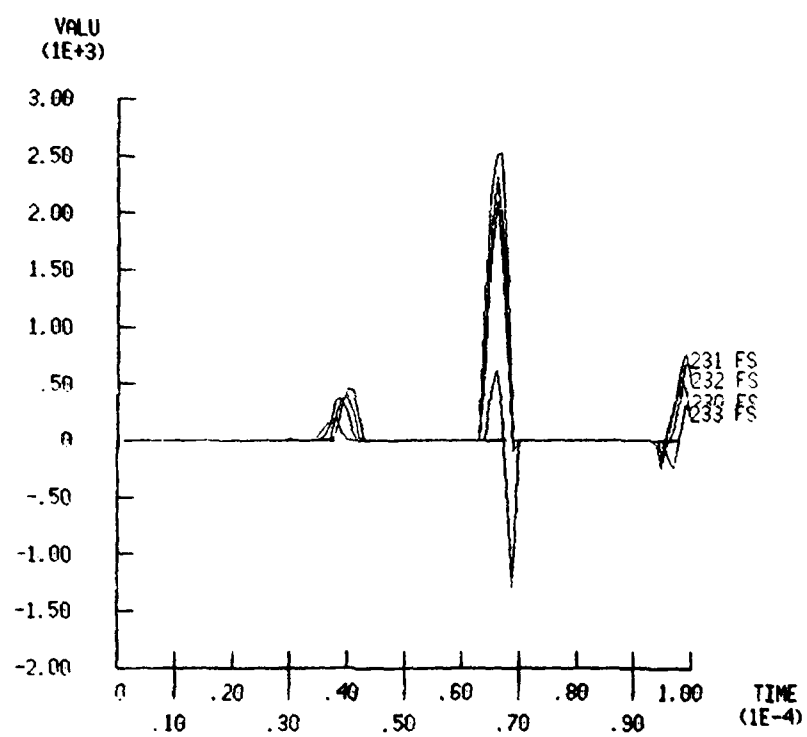
Figure 3.6.15. Gap Element Shear Force

57

The response of the reversed step joint model follows the behavior of the outside notched cylinder as far transmission coefficient is concerned. This is because both models have the same remaining cross-sectional area at the discontinuity. Both models transmit the same percentage of potential peak stress across the discontinuity.

Figure 3.6.16 shows a stress level of 53,000 psi in each of the five elements through the wall of the cylinder at a point below the joint. Figure 3.6.17, which are the stress histories of four elements well above the joint, indicate a peak transmitted stress of 54,000 psi, or 102 percent of the incident wave's peak stress. The model of the bimetallic cylinder with a plane joint predicts a maximum transmitted stress of 77,400 psi or 146 percent of the incident wave. Thus, the transmission coefficient is therefor 54,000/77,400 or approximately 70 percent, analagous to the outside-notched cylinder with the same remaining area at the discontinuity.

Finally, the stress patterns of the two step-jointed models are anti-symmetric due to the reversal of the joint. This phenomenon is also characteristic of the two notched cylinder models.

Figure 3.6.16. Stress Histories of a Row of Elements
Below the Joint

Figure 3.6.17. Stress Histories of a Row of Elements
Above the Joint

60

CHAPTER 4

CONCLUSIONS

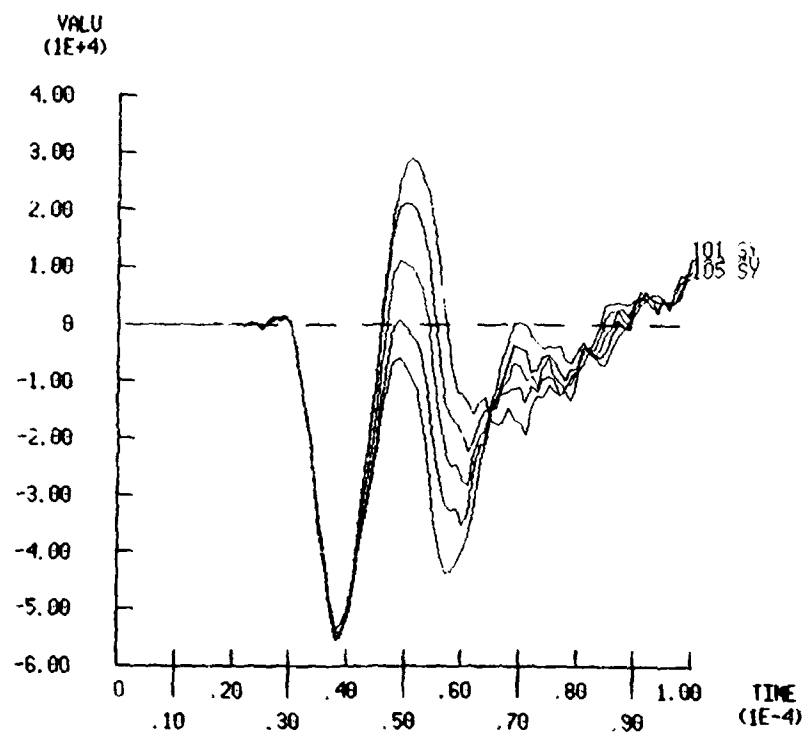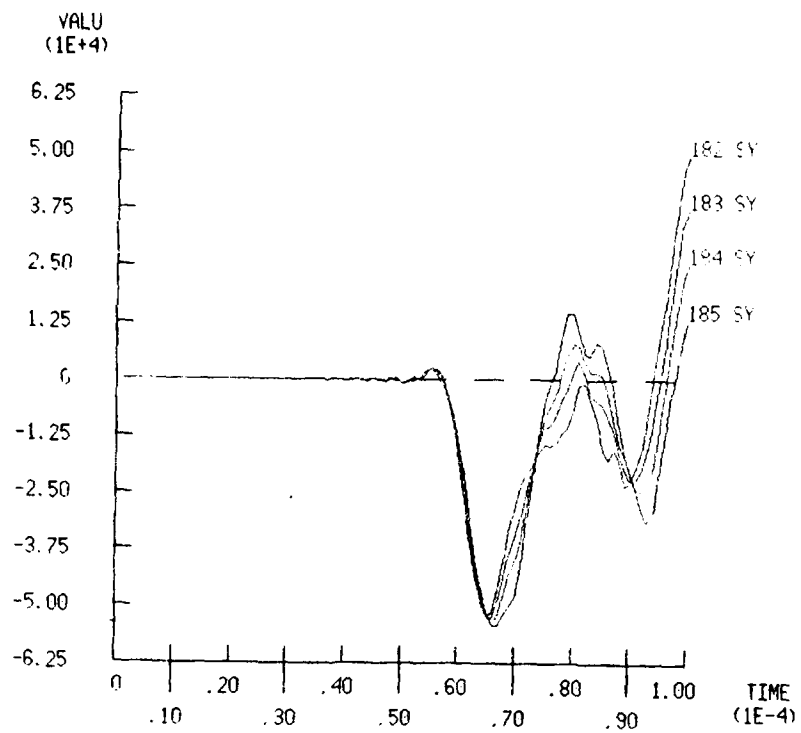The effect of a stress wave on a bi-metallic step joint between two cylinders are the production of localized elevated stresses through the wall thickness. These stress patterns indicate a steep gradient through the thickness of the aluminum flange producing a bending moment. Stresses in the steel flange produce a barreling effect. The direction of bending is such that the vertical interface tends to separate, which could be related to certain observed failures of cylindrical structures resulting from impact loading.

The ANSYS finite element program can be used to study stress wave propagation in complex structures. However obtaining useful results requires the ability to recognize and account for certain idiosyncratic aspects of the program. A generous distribution of mass points is required for structures with material and geometric discontinuities. The abbreviated analysis, which converges orders of magnitude more quickly, is accurate only for structures of simple, uniform geometry.

This study introduces the concept of transmission coefficient across material and geometric discontinuities on a variety of hollow cylinders subjected to a transient stress pulse. Hollow cylinders with only a material discontinuity (interface between different materials) exhibit a change in the peak value of the stress wave, as it crosses the interface, which is related to the ratio of material densities. The transmission coefficient for cylinders with geometric discontinuities, such as the non-closing notch, is not directly proportional to the remaining connected cross-sectional area. For this type discontinuity, it has been shown that the removal of 74 percent of the cross-sectional area by notching a hollow cylinder, results in the attenuation of only 50 percent of the maximum possible wave energy. This can be useful to the design engineer who is tasked to design a joint capable of supporting stress waves.

The attenuation of stress waves requires a sufficiently large notch for the purpose of obtaining a low transmission coefficient. However, the tradeoff is the elevated stresses in the remaining connected region. In contrast, if the the objective of th design is to reduce stresses in the connected region, it can be made larger in cross-sectional

61

area than the mating section, since the stresses in each section are not distributed in proportion to area. For example, to achieve nearly equal stresses in the material on either side of the vertical interface, the distribution of area might be two thirds for the connected region and one third for the mating part, depending on material properties.

Another notable phenomenon of hollow cylinders subjected to a transient stress pulse is that they exhibit different stress and displacement responses than do solid bars. Some of the wave energy in a hollow cylinder is transferred to initiate radial vibration, thus reducing the peak stress of the wave. Solid bars do not vibrate radially and therefore the peak stress of the wave is greater. However, since solid bars obey plane strain relationships, the wave speed is approximately five percent lower than in a thin-walled cylinder, whose wave speed closely follows that in a sheet which behaves in plane stress.

APPENDIX

REVIEW OF ELEMENTARY STRESS WAVE ANALYSIS

This section provides some background theory and on stress waves which was used in Chapter 4. The predicted response of the structure to stress waves was compared to the following relationships.

Stress waves were initially studied in the nineteenth century by such investigators as Stokes, Poisson, Kelvin and Rayleigh. Their theoretical studies remained untested by measurement until the early nineteen hundreds when measurement techniques first emerged. A renewed interest in the subject since then has resulted in numerous papers, books and articles from which most of the work in this section is drawn.

Rigid body dynamics assumes that when a certain point on a structure is acted upon by a force, the entire body is set into motion at the same instant. This type of analysis is sufficient for most cases of stress analysis. However, when the applied load is impulsive in nature and of duration smaller than the time it takes an acoustic wave to traverse the structure stress waves must be considered. The first step taken to study stress waves through the bi-metallic cylinder was to determine the wave velocity through the materials. The literature states that the wave velocity is dependent not only on density and modulus but also on geometry and boundary conditions, i.e. bar, plate, semi-infinite solid and lateral constraints. Kolsky [1] develops an expression for wave speed in a bar made of a linear, isotropic solid in the following manner: Using Hooke's law for an isotropic elastic solid the state of stress and strain can be expressed by six relationships:

$$\sigma_{xx} = \lambda\Delta + 2\nu\varepsilon_{xx} \quad \sigma_{yy} = \lambda\Delta + 2\nu\varepsilon_{yy} \quad \sigma_{zz} = \lambda\Delta + 2\nu\varepsilon_{zz} \quad (A1)$$

$$\sigma_{yz} = \nu\varepsilon_{yz} \qquad \sigma_{zx} = \nu\varepsilon_{zx} \qquad \sigma_{xy} = \nu\varepsilon_{xy}$$

where $\Delta = \varepsilon_{xx} + \varepsilon_{yy} + \varepsilon_{zz}$. The following differential equation represents the condition for dynamic equilibrium in the x-direction.

Expressing the stresses in terms of strains using equation (A1) gives:

$$\rho \frac{\partial^2 u}{\partial t^2} = \frac{\partial \sigma_{xx}}{\partial x} + \frac{\partial \sigma_{xy}}{\partial y} + \frac{\partial \sigma_{xz}}{\partial z}$$ (A2)

Substituting for σ_{xx}, σ_{yy}, σ_{zz} the relationships $\lambda \Delta + 2\nu \varepsilon_{xx}$, $\nu \varepsilon_{xy}$, and $\nu \varepsilon_{xz}$ respectively from elasticity gives:

$$\rho \frac{\partial^2 u}{\partial t^2} = \frac{\partial}{\partial x} (\lambda \Delta + 2\mu \varepsilon_{xx}) + \frac{\partial}{\partial y} (\mu \varepsilon_{xy}) + \frac{\partial}{\partial z} (\mu \varepsilon_{xz})$$ (A3)

then,
$$\rho \frac{\partial^2 u}{\partial t^2} = (\lambda + 2\nu) \nabla^2 u$$ (A4)

where
$$\nabla^2 = \frac{\partial^2}{\partial x^2} + \frac{\partial^2}{\partial y^2} + \frac{\partial^2}{\partial z^2}$$ (A5)

Similar expressions apply in a like manner to the y- and z-directions. Let $c_1 = \sqrt{(\lambda + 2\nu)/\rho}$ then this differential equation has the general solution of:

$$u = f(x + c_1 t) + F(x - c_1 t)$$ (A6)

where the first expression on the right is a wave travelling in the positive x-direction and the other expression is a wave travelling in the negative x-direction. The functions f and F describe the shape of the wave. At this point the term "particle velocity" is introduced. It is assumed that when a stress wave reaches the region under consideration, it sets all particles of matter in the region into motion in the direction of the wave. If attention is focused on only one of the functions, F (the result of two bars colliding and only one bar is examined, for example), the particle velocity u' is expressed as:

$$u' = \frac{\partial u}{\partial t} = - c_1 F'(x - c_1 t)$$ (A7)

Then, following Timoshenko [10], the kinetic energy for an element dx dy dz in the x-direction can be expressed as:

64

$$\frac{1}{2}\rho \, dxdydz \, (\partial u/\partial t)^2 = \frac{1}{2}\rho \, dxdydz * c_1^2 * (F'(x - c_1 t))\text{(A8)}$$

The potential energy, or strain energy, are given by:

$$V_0 \, dxdydz = - c_1 (F'(x - c_1 t)) \, dxdydz \qquad \text{(A9)}$$

where V_0 is the strain energy per unit volume and the strain components are:

$$\varepsilon_x = \frac{\partial u}{\partial x} = F'(x - c_1 t), \quad \varepsilon_y = \varepsilon_z = 0 \; .$$

The condition tnat ε_y and e_z are zero implies that tnese relationsnips are developed for tne case of uniaxial strain, whereby lateral motion is restricted such as for tne interior of thick solids or an infinite medium. For tne case of a bar or any shape whose lateral surface is free, as long as eacn slice of the cross-section benaves in simple tension, and the axial strain is a function of x and t then

$$\sigma_x = E\varepsilon_x \qquad \text{(A10)}$$

and the equation of motion is:

$$\frac{\partial^2 u}{\partial t^2} = c^2 \frac{\partial^2 u}{\partial x^2} \qquad \text{(A11)}$$

where $\qquad c = \sqrt{(E/\rho)} \qquad$ (A12)

For sections of solid that are are neitner thick nor tnin tne speed of a stress wave snould be somewhere in between c_1 and c, depending on the location of the elemental section. The value of c_1 is somewhat nigner than c and is computed from:

$$\frac{E(1 - \nu)}{(1 + \nu)(1 - 2\nu)\rho}. \qquad \text{(A13)}$$

It is difficult to judge wnetner a hollow cylinder benaves in uniaxial stress or uniaxial strain or somewhere in between. If the Poisson effect is present, whereby negative axial stress causes positive axial strain (lateral surfaces free to expand) the wave speed would tnen be the acoustic velocity.

The effect of a stress wave on a bi-metallic cylinder with a plane joint is next examined. If the interface between tne two cylinders is subjected to a stress wave, part of tne stress would be

transmitted through the joint and part would be reflected back depending on the respective densities. Rinehart [2] takes the particle velocity approach. A stress wave passing through reference line A at time t is depicted in Figure A.1. At time t + dt the wave has moved to reference line B. During the time dt, the stress has acted on the region between A and B imparting the impulse $\sigma_x dt$ to the region. Since the cross-sectional area and the density are assumed to be constant in the direction of travel, application of Newton's second law, namely impulse = change in momentum, the following relationship applies:

$$\sigma_x dt = \rho V_x dx = \rho V_x c_1 dt \qquad (A14)$$

Dividing through by dt and recognizing that $c_1 = dx/dt$ (c_1 is used instead of c because of constant cross-section, $\varepsilon_y = \varepsilon_z = 0$) the relation:

$$\sigma_x = \rho c_1 V_x \qquad (A15)$$

When a wave meets a normal interface between two materials, the particle velocities and the stress on either side of the interface must be equal, otherwise the law of conservation of momentum would be violated and the joint would separate due to momentum transfer. Also, displacement continuity must exist. The joint in the present case is considered to be permanently bonded. Thus, the following relationships apply for a wave meeting an interface with normal incidence:

$$\sigma_I + \sigma_R = \sigma_T \qquad (A16)$$

$$V_I + V_R = V_T \qquad (A17)$$

where σ is the stress, V is the particle velocity and and the subscripts I, R, and T are the incident, reflected, and transmitted values. Equation (A16) obeys the fundamental law of hydrostatic pressures and provided that only normal incidence is considered it also holds for solids. Equation (A17) is from continuity relationships. If (A15) is solved for V and substituted into (A17) for each of the three waves, this gives:

$$\frac{\sigma_I}{\rho c_1} - \frac{\sigma_R}{\rho c_1} = \frac{\sigma_T}{\rho' c_1'} \qquad (A18)$$

where the primes indicate the second medium. solving (A16) and (A18) simutaneously first for σ_T, then for σ_R gives:

66

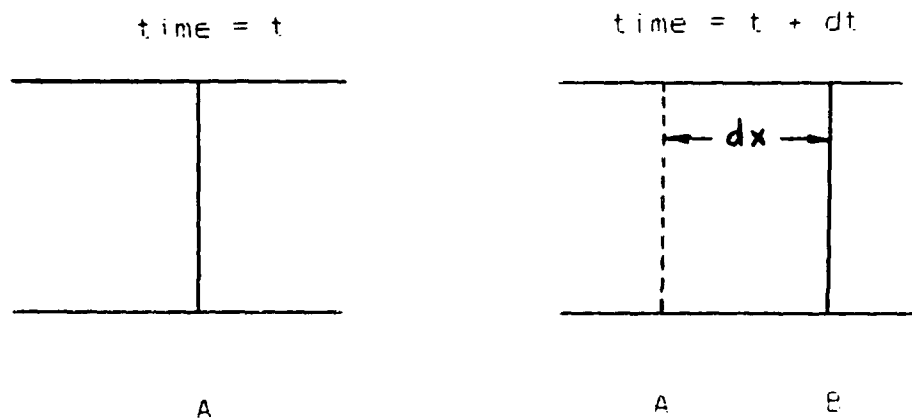time = t   time = t + dt

A   A   B

Figure A.1. Schematic Representation of a Stress Wave

$$\sigma_T = 2\sigma_I(\rho'c_1'/(\rho'c_1' + \rho c_1)) \tag{A19}$$

and $$\sigma_R = \sigma_I((\rho'c_1' - \rho c_1)/(\rho'c_1' + \rho c_1')) \tag{A20}$$

The ratio of transmitted to reflected stress can then be obtained by dividing (A19) by (A20) giving:

$$\sigma_T/\sigma_R = 2\rho'c_1'/(\rho'c_1' - \rho c_1) \tag{A21}$$

after having made suitable reductions. If the medium is aluminum and medium' is steel then σ_T/σ_R is 3.17. σ_R is calculated to be +.46 times the incident wave which means that a compression wave would reflect as compression wave at 46 per cent of the initial value. The transmitted stress would show a gain in amplitude of 46 per cent or a total of 1.46 times the incident wave. If the two waves were added together, viz. 1.46 + (-.46), the value of 1.0 would result, thus demonstrating conservation of energy. The algebraic sign indicates the direction of the wave, not the magnitude sign.

REFERENCES

[1]   Kolsky, H.
      Stress Waves in Solids
      Dover Publications, 1963

[2]   Rinehart, J.S.
      Stress Transients in Solids
      Hyperdynamics, 1975

[3]   Hopkins, A.K. and Chou, P.C.
      Dynamic Response of Materials to Intense Impulsive
      Loading
      Air Force Materials Laboratory, 1973

[4]   Yong, K.H. and Atkins, K.J.
      "Generation of Elastic Stress Waves at a T-Junction of
      Square Rods" Journal of Sound and Vibration, June 4,
      1983 p 431-436

[5]   O'Neill, J.P. and Tirman, C.J.
      "A Simple Device for the Attenuation of Longitudinal
      Elastic Stress Waves" U.S. Naval Research Laboratory
      Shock and Vibration Bulletin, December 5, 1969 p 157

[6]   Gallagher, R.H.
      Finite Element Analysis Fundamentals
      Prentice-Hall, 1975

[7]   Boresi, A.P., Sidebottom, O.M., Seely, F.B., Smith,
      J.O. Advanced Mechanics of Materials
      John Wiley & Sons, Inc., 1978

[8]   Kohnke, P.C.
      ANSYS Theoretical Manual
      Swanson Analysis Systems, Inc., 1983

[9]   Fung, Y.C.
      Foundations of Solid Mechanics
      Prentice-Hall, 1965

[10] Timoshenko, S.P., and Goodier, J.N.
      Theory of Elasticity
      Prentice-Hall, 1970

DISTRIBUTION LIST

12   Administrator
Defense Technical Info Center
ATTN: DTIC-DDA
Cameron Station
Alexandria, VA 22304-6145

1   HQDA (SARD-TR)
Washington, DC 20310-0001

1   Commander
US Army Materiel Command
ATTN: AMCDRA-ST
5001 Eisenhower Avenue
Alexandria, VA 22333-0001

1   Commander
US Army Laboratory Comi
ATTN: AMSLC-DL
Adelphi, MD 20783-1145

2   Commander
Armament RD&E Center
US Army AMCCOM
ATTN: SMCAR-MSI
Picatinny Arsenal, NJ 07806-5000

2   Commander
Armament RD&E Center
US Army AMCCOM
ATTN: SMCAR-TDC
Picatinny Arsenal, NJ 07806-5000

1   Director
Benet Weapons Laboratory
Armament RD&E Center
US Army AMCCOM
ATTN: SMCAR-LCB-TL
Watervliet, NY 12189-4050

1   Commander
US Army Armament, Munitions and
Chemical Command
ATTN: SMCAR-ESP-L
Rock Island, IL 61299-5000

1   Commander
US Army Aviation Systems Command
ATTN: AMSAV-DACL
4300 Goodfellow Blvd.
St. Louis, MO 63120-1798

1   Director
US Army Aviation Research and
Technology Activity
Ames Research Center
Moffett Field, CA 94035-1099

1   Commander
US Army Missile Command
ATTN: AMSMI-AS
Redstone Arsenal. AL 35898-5010

1   Commander
US Army Tank Automotive Command
ATTN: AMSTA-TSL (Technical Library)
Warren, MI 48397-5000

1   Director
US Army TRADOC Analysis Command
ATTN: ATAA-SL
White Sands Missile Range, NM 88002-5502

1   Commandant
US Army Infantry School
ATTN: ATSH-CD-CSO-OR
Fort Benning, GA 31905-5660

1   AFWL/SUL
Kirtland AFB, NM 87117-5800

1   Air Force Armament Laboratory
ATTN: AFATL/DLODL
Eglin AFB, FL 32542-5000

1   Director
Defense Advanced Research Projects Agency
1400 Wilson Boulevard
Arlington, VA 22209

1   Commander
US Army Materiel Command
ATTN: AMCDMD-ST
5001 Eisenhower Avenue
Alexandria, VA 22333-0001

1   Commander
US Army Materiel Command
ATTN: DRCLDC
5001 Eisenhower Avenue
Alexandria, VA 22333

6   Commander
USA AMCCOM, ARDEC
ATTN: SMCAR-CC (Mr. Barrieres)
SMCAR-CCH (R. Price)
SMCAR-CCH (S. Musalli)
SMCAR-CCH (L. Rosendorf)
SMCAR-CCH (B. Konrad)
SMCAR-CCH (E. Fennell)
Picatinny Arsenal, NJ 07801-5000

1   Commander
USA AMCCOM, ARDEC
ATTN: SMCAR-CCL
Picatinny Arsenal, NJ 07801-5000

DISTRIBUTION LIST

No of Copies	Organization
5	Commander USA AMCCOM, ARDEC ATTN: SMCAR-FS (H. Garrer) SMCAR-FFS SMCAR-FSP SMCAR-FSA (R. Wrenn) SMCAR-FSA (T. Gura) Picatinny Arsenal, NJ 07801-5000
1	Commander USA AMCCOM, ARDEC ATTN: SMCAR-TD (T. Davidson) Picatinny Arsenal, NJ 07801-5000
2	Commander USA AMCCOM, ARDEC ATTN: SMCAR-AE SMCAR-AE (M. Weinstock) Picatinny Arsenal, NJ 07801-5000
2	Commander USA AMCCOM, ARDEC ATTN: SMCAR-FS (R. Botticelli) Picatinny Arsenal, NJ 07801-5000
3	Director USA AMCCOM, ARDEC Benet Weapons Laboratory ATTN: SMCAR-CCB-TL SMCAR-CCB (L. Johnson) SMCAR-CCB-R (G. D'Andrea) Watervliet, NY 12189
2	Director USA AMCCOM, ARDEC Benet Weapons Laboratory ATTN: SMCAR-CCB-RA (T. Simkins) SMCAR-CCB-D (J. Zweig) Watervliet, NY 12189
1	Commander USA AMCCOM, ARDEC ATTN: Army Fuze Management Project Office SMCAR-FU Picatinny Arsenal, NJ 07801-5000
1	Commander USA AMCCOM, ARDEC ATTN: Development Project Office for Selected Ammunitions SMCAR-DP Picatinny Arsenal, NJ 07801-5000

No of Copies	Organization
1	Commmander USA AMCCOM, ARDEC ATTN: Product Assurance Directorate SMCAR-QAR-RIB, D. Inhof Picatinny Arsenal, NJ 07801-5000
1	Commander USA AMCCOM, ARDEC ATTN: SMCAR-ESP-L, Technical Library Rock Island, IL 61299
1	Commander USA Aviation Research and Development Command ATTN: AMSAV-E 4300 Goodfellow Boulevard St. Louis, MO 63120
1	Director USA Air Mobility Research and Development Laboratory Ames Research Center Moffett Field, CA 94035
1	Director USA Research and Technology Laboratories (AVRADCOM) Ames Research Center Moffett Field, CA 94035
1	Commander USA Communications Command ATTN: AMSEL-ED Fort Monmouth, NJ 07703
1	Commander USA Electronics Research and Development Command Technical Support Activity ATTN: DELSD-L Fort Monmouth, NJ 07703-5301
1	Commander USA Harry Diamond Labs ATTN: DELHD-TA-L 2800 Powder Mill Road Adelphi, MD 20783
1	Commander USA Missile Command RD&E Center ATTN: AMSMI-RD Redstone Arsenal, AL 35898
1	Commander USA Missile Command ATTN: AMSMI-R Redstone Arsenal, AL 35898

DISTRIBUTION LIST

No of Copies	Organization	No of Copies	Organization
1	Commander USA Missile Command ATTN: AMSMI-RBL Redstone Arsenal, AL 35898	2	Director USA Mechanics and Materiels Research Center ATTN: Director AMXMR-ATL Watertown, MA 02172
1	Commander USA Missile Command ATTN: AMSMI-RBL Redstone Arsenal, AL 35898	2	Commander USA Materials and Mechanics Research Center ATTN: J. Mescall (Technical Library) Watertown, MA 02172
1	Commander USA Natick Research and Development Command ATTN: DRXRE, H. Sieling Natick, MA 01762	1	Commander Naval Air Systems Command ATTN: AIR-604 Washington, DC 20360
1	Commander USA Research Office P.O. Box 12211 Research Triangle Park, NC 27709	1	Commander Naval Ordnance Systems Command ATTN: ORD-9132 Washington, DC 20360
1	Commander USA Research Office P.O. Box 12211 ATTN: Engineering Division Research Triangle Park, NC 27709	1	Commander Naval Sea Systems Command Washington, DC 20362
1	Commander USA Research Office ATTN: J. Chandra Research Triangle Park, NC 27709	1	Commander Naval Ship Systems Command Washington, DC 20360
2	Project Manager USA AMCCOM, ARDEC Cannon Artillery Weapons System ATTN: AMCPM-CAWS AMCPM-CAWS-A (R. DeKleine) Picatinny Arsenal, NJ 07801-5000	1	Superintendent Naval Postgraduate School ATTN: Director of Library Monterey, CA 93940
		1	Commander Naval Research Laboratory Washington, DC 20375
1	Project Manager Nuclear Munitions ATTN: AMCPM-NUC Picatinny Arsenal, NJ 07801-5000	1	Commander Naval Ship Research and Development Center Bethesda, MD 20084
1	Project Manager Tank Main Armament Systems ATTN: AMCPM-TMA Picatinny Arsenal, NJ 07801-5000	1	Commander Naval Surface Weapons Center ATTN: G-13, W.D. Ralph Dahlgren, VA 22448
1	Product Manager M110E2 Weapon System, DARCOM ATTN: AMCPM-M110E2 Rock Island, IL 61299	1	Commander Naval Surface Weapons Center ATTN: Code X211, Lib Silver Spring, MD 20910
		1	Commander Naval Weapons Center ATTN: Code 3431, Technical Library China Lake, CA 93555

DISTRIBUTION LIST

USER EVALUATION SHEET/CHANGE OF ADDRESS

This laboratory undertakes a continuing effort to improve the quality of the reports it publishes. Your comments/answers below will aid us in our efforts.

1. Does this report satisfy a need? (Comment on purpose, related project, or other area of interest for which the report will be used.) _____

    _____

    _____

2. How, specifically, is the report being used? (Information source, design data, procedure, source of ideas, etc.) _____

    _____

    _____

3. Has the information in this report led to any quantitative savings as far as man-hours or dollars saved, operating costs avoided, or efficiencies achieved, etc? If so, please elaborate. _____

    _____

    _____

4. General Comments. What do you think should be changed to improve future reports? (Indicate changes to organization, technical content, format, etc.) _____

    _____

    _____

BRL Report Number _____   Division Symbol _____

Check here if desire to be removed from distribution list. _____

Check here for address change. _____

Current address: Organization _____
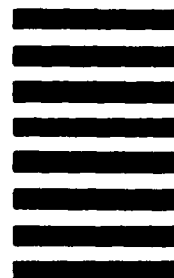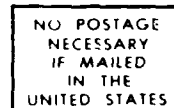   Address   _____
                                _____

------------------------------FOLD AND TAPE CLOSED-----------------------------

Director
U.S. Army Ballistic Research Laboratory
ATTN: SLCBR-DD-T(NEI)
Aberdeen Proving Ground, MD 21005-5066

||||||

OFFICIAL BUSINESS
PENALTY FOR PRIVATE USE $300

BUSINESS REPLY LABEL
FIRST CLASS   PERMIT NO 12062 WASHINGTON D C

POSTAGE WILL BE PAID BY DEPARTMENT OF THE ARMY

Director
U.S. Army Ballistic Research Laboratory
ATTN: SLCBR-DD-T(NEI)
Aberdeen Proving Ground, MD 21005-9989